Brain, Behavior, & Immunity - Health 28 (2023) 100568

Contents lists available at ScienceDirect

Brain, Behavior, & Immunity - Health

journal homepage: www.editorialmanager.com/bbih/default.aspx

Systemic Inflammation Causes Microglial Dysfunction With a Vascular AD phenotype

Praveen Bathini [a,1,**], Isabel Dupanloup [b], Elena Zenaro [c], Eleonora Terrabuio [c], Amrei Fischer [a], Edona Ballabani [a], Marie-Agnes Doucey [d], Lavinia Alberi [a,e,*]

[a] Department of Medicine, University of Fribourg, Fribourg, Switzerland
[b] Swiss Institute for Bioinformatics, Lausanne, Switzerland
[c] Department of Medicine, Section of General Pathology, University of Verona, Verona, Italy
[d] University of Lausanne, Lausanne, Switzerland
[e] Swiss Integrative Center for Human Health, Fribourg, Switzerland

ARTICLE INFO

Keywords:
Inflammation
PolyI:C
Brain aging
Microglia
Sporadic Alzheimer's disease
Vascular dementia

ABSTRACT

Background: Studies in rodents and humans have indicated that inflammation outside CNS (systemic inflammation) affects brain homeostasis contributing to neurodevelopmental disorders. Itis becoming increasingly evident that such early insults may also belinked to neurodegenerative diseases like late-onset Alzheimer's disease (AD). Importantly, lifestyle and stress, such as viral or bacterial infection causing chronic inflammation, may contribute to neurodegenerative dementia. Systemic inflammatory response triggers a cascade of neuroinflammatory responses, altering brain transcriptome, cell death characteristic of AD, and vascular dementia. Our study aimed to assess the temporal evolution of the pathological impact of systemic inflammation evoked by prenatal and early postnatal peripheral exposure of viral mimetic Polyinosinic:polycytidylic acid (PolyI:C) and compare the hippocampal transcriptomic changes with the profiles of human post-mortem AD and vascular dementia brain specimens.

Methods: We have engineered the PolyI:C sterile infection model in wildtype C57BL6 mice to achieve chronic low-grade systemic inflammation. We have conducted a cross-sectional analysis of aging PolyI:C and Saline control mice (3 months, 6 months, 9 months, and 16 months), taking the hippocampus as a reference brain region, and compared the brain aging phenotype to AD progression in humans with mild AD, severe AD, and Controls (CTL), in parallel to Vascular dementia (VaD) patients' specimens.

Results: We found that PolyI:C mice display both peripheral and central inflammation with a peak at 6 months, associated with memory deficits. The hippocampus is characterized by a pronounced and progressive tauopathy. In PolyI:C brains, microglia undergo aging-dependent morphological shifts progressively adopting a phagocytic phenotype. Transcriptomic analysis reveals a profound change in gene expression throughout aging, with a peak in differential expression at 9 months. We show that the proinflammatory marker *Lcn2* is one of the genes with the strongest upregulation in PolyI:C mice upon aging. Validation in brains from patients with increasing severity of AD and VaD shows the reproducibility of some gene targets in vascular dementia specimens as compared to AD ones.

Conclusions: The PolyI:C model of sterile infection demonstrates that peripheral chronic inflammation causes progressive tau hyperphosphorylation, changes in microglia morphology, astrogliosis and gene reprogramming reflecting increased neuroinflammation, vascular remodeling, and the loss of neuronal functionality seen to some extent in human AD and Vascular dementia suggesting early immune insults could be crucial in neurodegenerative diseases.

* Corresponding author. Swiss Integrative Centre of Human Health, Passage du Cardinal 13B, CH-1700, Fribourg, Switzerland.
** Corresponding author.
E-mail addresses: pbathini@bwh.harvard.edu (P. Bathini), isabelle.dupanloup@sib.swiss (I. Dupanloup), elena.zenaro@univr.it (E. Zenaro), eleonora.terrabuio@univr.it (E. Terrabuio), amrei.fischer@unifr.ch (A. Fischer), edona.ballabani@unifr.ch (E. Ballabani), Marie-Agnes.Doucey@ichnossciences.com (M.-A. Doucey), lavinia.alberi@unifr.ch (L. Alberi).
[1] Brigham and Women's Hospital, Harvard Medical School (**present address**).

https://doi.org/10.1016/j.bbih.2022.100568
Received 9 August 2022; Received in revised form 12 November 2022; Accepted 26 November 2022
Available online 21 December 2022

1. Introduction

The central nervous system (CNS), once considered an immune-privileged site, is monitored by resident glial cells and circulating immune cells from the periphery. The crosstalk between neuronal and non-neuronal cells operates under homeostatic conditions for proper brain functioning (Sankowski et al. 2015). Systemic chronic low-grade inflammation (SCI) is primarily caused by microbial infections and metabolic dysfunction. This perturbs the brain's homeostasis and is implicated in many chronic diseases, including neurodegenerative dementia (Furman et al., 2019). The recent COVID-19 pandemic suggested a close relationship between viral infections and cognitive dysfunction (Zhou et al., 2021) with long-term memory deficits (Søraas et al., 2021) and associated vascular endothelial damage (Lee et al., 2021). Previous work has demonstrated that exposure to microbial pathogens (viruses, bacteria, fungi, etc) can potentiate neuroinflammation and accelerate neuropathological events (Sochocka et al. 2017). Spirochetes, Chlamydia Pneumoniae, Porphyromonas Gingivalis, and Herpes Simplex Viruses (HSV-1, HSV-2, and HHV-6) are enriched in the brains of Alzheimer's disease (AD) patients and their titer correlates with the progression of the disease (Fulop et al., 2018). The casual relationship between viral infection and the development of dementia has been recently supported by retrospective observational studies looking at the protective role of antiviral drugs for dementia (Tzeng et al., 2018). Recent studies indicated a stronger association between infectious diseases and vascular dementia than for AD (Sipilä et al., 2021). Interestingly, at least two reports show that viral infections are more recurrent in APOEε4 carriers, bearing a higher risk of dementia conversion with aging (Linard et al., 2020; Itzhaki and Wozniak 2006).

Late-onset AD affects people over 65 years of age and vascular dementia (VaD) accounts for the second most frequent mixed pathology with AD (Toledo et al., 2013; Lin et al., 2019; Santos et al., 2017) shows the involvement of both genetic and environmental factors. Underlying the pathogenesis of the disease, a large proportion of genetic factors, such as ABCA7, APOE, BIN1, CD2AP, CD33, CLU, CR1, HLA-DRB1, and SORL1 (Barber 2012) are immunological factors. Furthermore, APOE and SORL1 have been previously associated with Cerebral Amyloid Angiopathy (CAA) (Du et al., 2019) supporting vascular inflammation as a comorbidity factor accelerating the progression of AD (Thal et al., 2002). Many of these genes are associated with dysregulated microglial responses toward pathogenic stimuli. Haplodeficiency of ABAC7 impairs microglial CD14 expression, a pattern recognition receptor, and causes excessive amyloid accumulation and abnormal endosomal morphology in these resident immune cells (Aikawa et al., 2019). ApoE isoforms and its phospholipid composition regulate the expression of microglial receptors, chemotaxis, activation, phagocytosis and Aβ interaction with ApoE3 lipoproteins triggering a better microglial response than ApoE4 (Fitz et al., 2021). While different mutations are involved in the pathophysiology of AD, microglia are the key regulator and fulcrum in the neuroinflammatory response in neurodegeneration (Moore et al., 2019). Aging causes microglial senescence, inducing functional changes and thereby increasing neuroinflammatory responses. Age-associated increased in the expression of CD68, lipofuscin aggregation, reduced phagocytosis, reduced motility switch the microglial phenotype to shorter, thicker dendrites with fewer branches (Chen et al., 2021; Streit et al., 2004; Sierra et al., 2007).

Further, epidemiological studies indicate maternal infections as one of the priming events for chronic neuroinflammatory responses (Li et al., 2018), representing a major risk factor for neurodevelopmental disorders in the offspring (Conway and Brown 2019; Bilbo et al., 2018) and neurodegenerative diseases such as Parkinson's disease (Carvey et al., 2003) or late on-set AD (Hoeijmakers et al., 2016; Knuesel et al., 2014). Animal studies confirm that prenatal viral infection induces neuroinflammation and cognitive deficits (Ito et al., 2010) and that recurrent infections may cause an Alzheimer' s-like phenotype (Little et al., 2004; Dominy et al., 2019; De Chiara et al., 2019). Previous animal studies using PolyI:C (Polyinosinic:polycytidylic acid), a synthetic double-stranded RNA that induces viral-like inflammation through toll-like receptor 3 (TLR3) signaling (Ting 2001), reported that late prenatal viral-like immune activation was enough to induce chronic inflammation and predisposes the offspring to AD-like neuropathology (Kristic et al., 2012). This evidence was later rejected in a work showing that prenatal immune insults with PolyI:C can induce only transient inflammatory responses despite producing cognitive impairments in the injected mice (Giovanoli et al., 2015). Taking into consideration the evidence supporting a role for chronic inflammation in AD but also the discrepancies on the effect of viral immune challenge in the development of AD, we readapted the PolyI:C mouse model to achieve a chronic systemic inflammation in naive mice by two injections, one in late pregnancy and the second in the young adult offspring. In our experimental paradigm, the early second immune challenge bolus was hypothesized to achieve sustained chronic inflammation deviating from the original model (Krstic et al., 2012) that could not be replicated by other studies (Giovanoli et al., 2015). The newly optimized PolyI:C mouse model reveals long term systemic & central immune response resulting in a significant increase in tau phosphorylation, dynamic changes in microglial morphology, transcriptomic changes leading to increased lipid metabolism, vascular factors activation, and spatial memory deficits. Our findings further consolidate the link between an imbalance of the immune system and dementia (Morgan et al., 2019; Engelhart et al., 2004; Leung et al., 2013), with peripheral inflammation prompting central immune responses (Perry et al. 2007) and causing neurodegeneration in the long-term (Saeed et al., 2014).

2. Materials and Methods

2.1. Animals

Wildtype C57BL/6J mice were used for the study. Animal experimentation was approved by the animal experiment committee, University of Fribourg (Protocol no. 2016_32_FR registered 01/01/2017). The animals were fed ad libitum and housed in a room equipped with automatically controlled temperature (21–25 °C), humidity (50%), and a 12 h light/dark cycle. Hippocampal brain slices from 16 month old APP PS1dE9 mice were obtained from Dr. Cynthia Lemere, Brigham and Women's Hospital, and were processed for immunohistochemical analysis. The number of animals used is reported for each experiment in the figures' legend.

2.2. Ethical approval and consent to participate

Frozen Human tissue samples from the entorhinal cortex including the hippocampal area were procured from the Medical Research Council Brain Bank for Dementia Research, Oxford, UK, and Stanford brain bank. We received frozen hippocampal brain tissue samples from 9 controls, 5 moderate, and 10 Severe sporadic AD patients (Suppl. Table 1). The use of human tissue has been approved by the Ethical Commission of the Brain Bank for Dementia UK (OBB443 registered 1/05/2017 and OB344 registered 1/02/2014), Stanford (Stanford IRB), and the Ethical Commission from the Canton of Fribourg and Vaud (N. 325/14). Vascular dementia hippocampal specimens and healthy age-matched controls were obtained from the Netherlands Brain Bank (NBB. 1251). All experiments conducted on human tissue comply with the WMA Declaration of Helsinki.

2.3. Treatment

To investigate the early postnatal treatment and microglial priming the systemic PolyI:C challenges were optimized from the already existing model with PolyI:C (Krstic et al., 2012). Female C57BL/6J mice 6–8 weeks old were housed together with the males for mating. Vaginal plugs were assessed and pregnant mice with gestation day (GD) 17 were

injected intravenously (i.v.) with 5 mg/kg PolyI:C (Poly-inosinic-polycytidylic acid; P9582, Sigma, USA). Aliquots of 5 mg/ml were prepared by resuspending in the sterile 0.9% saline and were stored at −20 °C until further use. For control experiments sterile 0.9% saline was used. To mimic chronic or recurrent inflammatory responses to systemic viral infections like in humans, prenatally challenged offspring at 2.5 months were given a second immune challenge with an intraperitoneal (i.p.) PolyI:C injection at 20 mg/kg dose or sterile saline for the control experimental mice (Fig. 1A). For all the subsequent experiments adult male offspring were used in the study.

2.4. Behavioral experiments

In this work, we characterized age-related changes in the mice behavior throughout aging i.e., from young adulthood to aged mice. Anxiety was tested at 3, 6, 9, and 16 months of age in PP mice (Prenatal and Postnatal PolyI:C injected) and NN mice (Prenatal and Postnatal saline injected) using the Open field test registering the time spent in the center, while elevated O-maze was used at 3–6 months only recording both the time spent in the open unprotected arm and time spent in the light. Working memory was tested using the Y-maze alternation task and expressed as % of alternation and number of arm entries during a 5-minutes (min) exploration window according to previously published protocols (Crawley and Bailey 2008; Miedel et al., 2017). Behavioral tests were videotaped and videos were analyzed using Image J-built in macros for automated video-tracking (Supplementary Material and Methods) (Brai and Alberi 2015).

2.5. Tissue processing

Animals were first deeply anesthetized with pentobarbital sodium (100 mg/kg, i.p) and verified with toe pinch pain reflex. After the abdominal opening, mice were transcardially perfused with 0.9% sterile saline, brains were harvested and cut into two hemispheres. One hemisphere was dissected to collect the hippocampus and further dissected in an ice-cold saline solution to obtain the Corpus Ammonis (CA) fields, removing the dentate gyrus (Brai et al., 2015). The tissue samples were collected into eppendorfs and were flash-frozen in liquid nitrogen and stored at −80 °C until further use. The other hemisphere was post-fixed in 4% PFA for 1 day, followed by immersion in 30% sucrose at 4 °C and then embedded in an OCT block for cryosectioning at 35 μm thickness (Leica, Germany) and used for histological studies.

2.6. Plasma collection

The whole blood collected via cardiac puncture was transferred into the EDTA-coated eppendorfs. Cells were separated from the plasma by centrifugation for 15 min at 2000x *g* at 4 °C before extracting the plasma. The plasma samples were then stored at −80 °C until further use.

2.7. Isolation of leukocytes from mouse tissues and flow cytometry

Blood: Mice were anesthetized via isoflurane inhalation. Blood samples were collected through a retro-orbital non-surgical procedure by sodium heparinized capillaries. Dextran 1% and Heparin 10 U/ml were added to the blood in a 1:1 ratio. After erythrocytes sedimentation [1 hour (h)], the overlying supernatant plasma-dextran suspension of leukocytes was washed in 1X PBS. Red blood cell lysis was performed adding 3 ml of NaCl 0.2% for 40 seconds and then 7 ml of NaCl 1.2%. Next, cells were washed and stained.

Brain: Mice were anesthetized and quickly perfused through the left cardiac ventricle by injection of cold PBS 1X Ca_2Mg_2 1 mM. After meninges removal, brains were collected. Mechanical digestion through gentleMACS™ Octo Dissociator (Miltenyi Biotec) and subsequent enzymatic digestion with 2 mg/ml of collagenase (C0130; Sigma-Aldrich, USA) and 40 U/ml of DNase (EN0521; Invitrogen, Life Technologies, USA) at 37 °C for 45 min in water bath were performed. Cells were isolated by passing the digested tissue through a 70-mm cell strainer, resuspended in 30% Percoll (GE Healthcare, USA), and loaded onto 70% Percoll (GE Healthcare, USA). After centrifugation at 2500 rpm for 20 min at 4 °C, cells were removed from interphase, washed, and stained.

Cells were treated with an antibody against Fc receptor [anti-mouse CD16/32, Clone: 2.4G2; Becton Dickinson (BD), USA] and labeled with BD Horizon Brilliant™ Stain Buffer (BD, USA) to improve staining quality and with 2.5 ml per sample of each of the following anti-mouse mAbs: Ly6G BB515 (Clone: 1A8; BD, USA), CD45 BV786 (Clone, 104 RUO; BD, USA), CD11b BV421 (Clone: R1-2; BD, USA), F4/80 (Clone: T45-2342 RUO; BD, USA), CD11c BV 605 (Clone: HL3; BD, USA), Siglec F PE (Clone: S17007L; BD, USA), B220 APC (Clone: RA3-6B2 RUO; BD, USA). Cells were stained for 15 min at 4 °C in the dark according to the manufacturer's instructions. After washing, cells were incubated with 7AAD (BioLegend, USA) fluorescent intercalator for 5 min at 4 °C in the dark. Samples were acquired through LSRFortessa X-20 (BD, USA). Data were analyzed through FlowJo™ Software. In particular, after doublets removal, $7AAD^-$ alive cells were selected. A specific gating strategy was used to identify subpopulations of leukocytes in blood and brain samples. The following $CD45^+$ cell populations were detected and analyzed: $Ly6G^+$ $CD11b^+$ $B220^-$ Neutrophils, Siglec F^+ $CD11b^-$ $CD11c^-$ Eosinophils, $F4/80^+$ $CD11b^+$ $SiglecF^-$ Monocytes. Using the DownSample Plugin developed by FlowJo™ (https://docs.flowjo.com/seqgeq/dimensionality-reduction/downsample/), the number of $CD45^+$ events in the data matrix was reduced to a maximum of 30.000.

Table 1
Plasma inflammatory panel in aging PP and NN mice.

Age	Group	Chemokine (pg/ml)	Inflammatory cytokines (pg/ml)		
		MCP-1	IL-6	TNF-α	IL-10
3 months	NN	11.1 ± 0.7	7.1 ± 0.2	3.8 ± 0.3	2.7 ± 0.2
	PP	19.8 ± 1.9	8.3 ± 0.3	3.3 ± 0.2	7.7 ± 0.7
	Fold change	1.8*	1.2	0.9	2.9*
6 months	NN	12.1 ± 3.4	2.4 ± 0.2	3.2 ± 0.2	4.1 ± 1.6
	PP	29.8 ± 11.9	15.8 ± 10.6	6.8 ± 0.7	12.0 ± 3.6
	Fold change	2.5*	6.5**	2.1**	2.9**
9 months	NN	35.7 ± 26.9	243.4 ± 187.5	8.9 ± 0.7	16.4 ± 4.7
	PP	17.2 ± 8.4	1464.2 ± 184.5	8.3 ± 0.2	9.1 ± 1.9
	Fold change	0.5	6.1**	0.9	0.6
16 months	NN	2.5 ± 1.0	6.5 ± 0.1	8.0 ± 0.3	10.5 ± 2.1
	PP	2.2 ± 0.5	6.9 ± 0.3	7.9 ± 0.2	4.7 ± 1.7
	Fold change	0.9	1.1	1.0	0.5

Data are represented as mean ± SEM. NN = prenatal& postnatal saline injected controls, PP = prenatal and postnatal PolyI:C treated mice. 3 months (NN = 4, PP = 4), 6 months (NN = 8, PP = 8), 9 & 16 months (NN, PP = 5 each). *$p < 0.05$, **$p < 0.01$ versus control group, two-way ANOVA followed by Bonferroni`s post hoc test.

2.8. Bead-based immunoassay

To study the PolyI:C effect on plasma inflammatory profile, we measured chemokines IL-6, IL-10, MCP-1, and TNF-α using the premixed inflammation panel (PN: C282251A, Aimplex Biosciences, USA) according to the manufacturer's instructions. Briefly, 45 µl of the capture bead working solution, 30 µl of assay buffer, and 15 µl of the sample were incubated on the shaker (700 rpm) for 60 min at room temperature. After 3 washes with 100 µl washing buffer, 25 µl of biotinylated antibody working solution was added and incubated on the shaker for 30 min at room temperature with protection from light. After 3 washes, 25 µl of streptavidin-phycoerythrin working solution was added, shaken for 20 min in the dark. Finally, the beads were resuspended on 150 µl of 1x reading buffer and read on Flow Cytometry Analyzer (LSR-IIa; BD, USA) acquiring about 50 events per chemokine. The FCS files were analyzed on the open access Flowing software (http://flowingsoftware.btk.fi/) and the cytokines' and chemokines' levels were determined based on 5-parameter logistic curve fitting.

2.9. Nucleic acid and protein extraction

Fresh frozen hippocampal tissue specimens from mice and humans are stored at −80 °C until utilized for RNA extraction using peqGOLD TriFast™ (peqGOLD, Germany) according to the manufacturer's instructions to obtain RNA and proteins. The RNA pellet was extracted from the aqueous phase, air-dried, resuspended in 25 µl of nuclease-free water (Promega). The concentration of the RNA samples was measured using the Qubit 3.0 Fluorometer (High sensitivity, Invitrogen) and stored at −80 °C until further use. Proteins were extracted from the organic phase, cleaned with Ethanol, and the dried pellet resuspended with a 150 µl buffer containing 8M Urea in 4% (w/v) CHAPS and protease inhibitor (1:100 Carl Roth, Germany). The protein concentrations were determined using the Bradford assay method (Roth, Germany), and later the samples were stored until use at −80 °C.

2.10. RNA library preparation and sequencing

Synthesis and amplification of cDNA were performed as per the Illumina TruSeq Stranded mRNA protocol. RNA extracted from the hippocampal specimens from all the age groups (3m, 6m, 9m, 16m) was used for this transcriptomics study. RNA integrity was determined with the Fragment Analyzer 5200 (Agilent). Samples with RNA integrity number (RIN) > 8 were used for the experiment. An input material of 1 µg of total RNA from each sample was used for library preparation with Illumina TruSeq Stranded mRNA kit (Cat: 20020595). Illumina TrueSeq Combinatorial dual (CD) indexes were used during the ligation, DNA fragments were enriched using the PCR to amplify the amount of DNA in the library. The quality of the libraries is determined using the Standard High sensitivity NGS Fragment analysis kit (DNF-474, 1–6000 base pair) on the Agilent Fragment analyzer (Agilent, USA), yielding approximately 260 bp size fragments. The cDNA libraries were pooled in equivalent amounts. The libraries were denatured and diluted using standard library quantification and quality control procedures recommended as per the NextSeqprotocol. For a sequencing control, the PhiX library was prepared and combined with the pooled prepared libraries. A final concentration of 1.5 pM library was sequenced on Illumina NextSeq 500 system (High output 150 cycles) to generate 20 millions of 2 × 75 bp pair-end reads per library.

2.11. Bioinformatics analysis

In brief, hippocampal paired-end libraries from all the age groups (3m, 6m, 9m, 16m) in the saline treated and PolyI:C treated mice (n = 3 each) were sequenced for the study. To generate the differentially expressed transcripts from the RNA sequencing data the following bioinformatics analysis pipeline was performed. 1) Remove adapter sequences and remove low quality (flanking N) bases from each read using cutadapt version 2.3; 2) Alignment of the reads to the reference genome using RNA-seq aligner STAR version 2.6; 3) Get basic alignment stats

Table 2
Validation of transcripts via qPCR in aging PP mice as compared to age-matched NN.

Age	Gene	Log2FC RNA-seq	FC qPCR	Regulation	Pathways& Functions	P value
3 months	*Lcn2**	–	−0.32	Down	Inflammatory signaling; dendritic spine pruning	0.02
	*Kcnj2**	–	1.01	–	Ionic conductance; slow inhibitory current	0.95
	*Egr2**	−0.1 (NS)	0.9	–	Early immediate gene	0.94
	*Plin4**	0.6 (NS)	3.1	–	Lipid metabolism	0.23
	Cacna1g	−0.6	0.9	–	Calcium channel	0.77
6 months	*Lcn2**	–	−0.6	–	Inflammatory signaling; dendritic spine pruning	0.70
	Glpr2	−3.7	−0.2	Down	Akt-mTOR; synaptic activity, neuroprotection	0.03
	Ide	0.5	1.6	–	Insulin signaling; Amyloid-® processing	0.16
	*Kcnj2**	0.1 (NS)	1.8	Up	Ionic conductance; slow inhibitory current	0.04
	*Egr2**	−0.68	−0.7	Down	IEG response; immune response	0.04
	*Plin4**	−0.23 (NS)	0.28	–	Lipid metabolism	0.49
9 months	*c-Jun*	−0.9	−1.8	Down	JNK3 pathway; IEG	0.05
	c-fos	−1.7	−3.2	Down	JNK3 pathway; IEG	0.002
	Notch1	−0.5	−2.5	Down	Notch signaling; synaptic plasticity	0.002
	*Kcnj2**	−0.7	−0.27	–	Ionic conductance; slow inhibitory current	0.35
	*Egr2**	−0.9	−0.5	Down	IEG response; immune response	0.02
	*Lcn2**	2.0	2.6	Up	Inflammatory signaling; dendritic spine pruning	0.05
	*Plin4**	2.7	1.8	–	Lipid metabolism	0.24
	Klf4	−2.1	−0.43	Down	Inflammation, vascular intergrity	0.01
	Cyp1b1	1.6	2.4	Up	Cell adhesion, angiogenesis	0.07
	Angptl4	1.7	2.4	Up	Vascular permeability Lipid homeostasis	0.02
16 months	*Kcnj2**	−0.8	−0.8	–	Ionic conductance; slow inhibitory current	0.36
	*Egr2**	−1.2(NS)	0.85	–	IEG response; immune response	0.3
	*Lcn2**	5.6	4.5	Up	Inflammatory signaling; dendritic spine pruning	0.04
	*Plin4**	1.8	2.3	Up	Lipid metabolism	0.03
	Klf4	0.02	−0.08	–	Inflammation, vascular intergrity	0.82
	Cyp1b1	1.0	1.45	–	Cell adhesion, angiogenesis	0.28
	Angptl4	1.0	1.1	–	Vascular permeability Lipid homeostasis	0.47

FC=Fold Change; NS = non-significant DEG; * Shared genes with progressive changes in the PP versu NN.

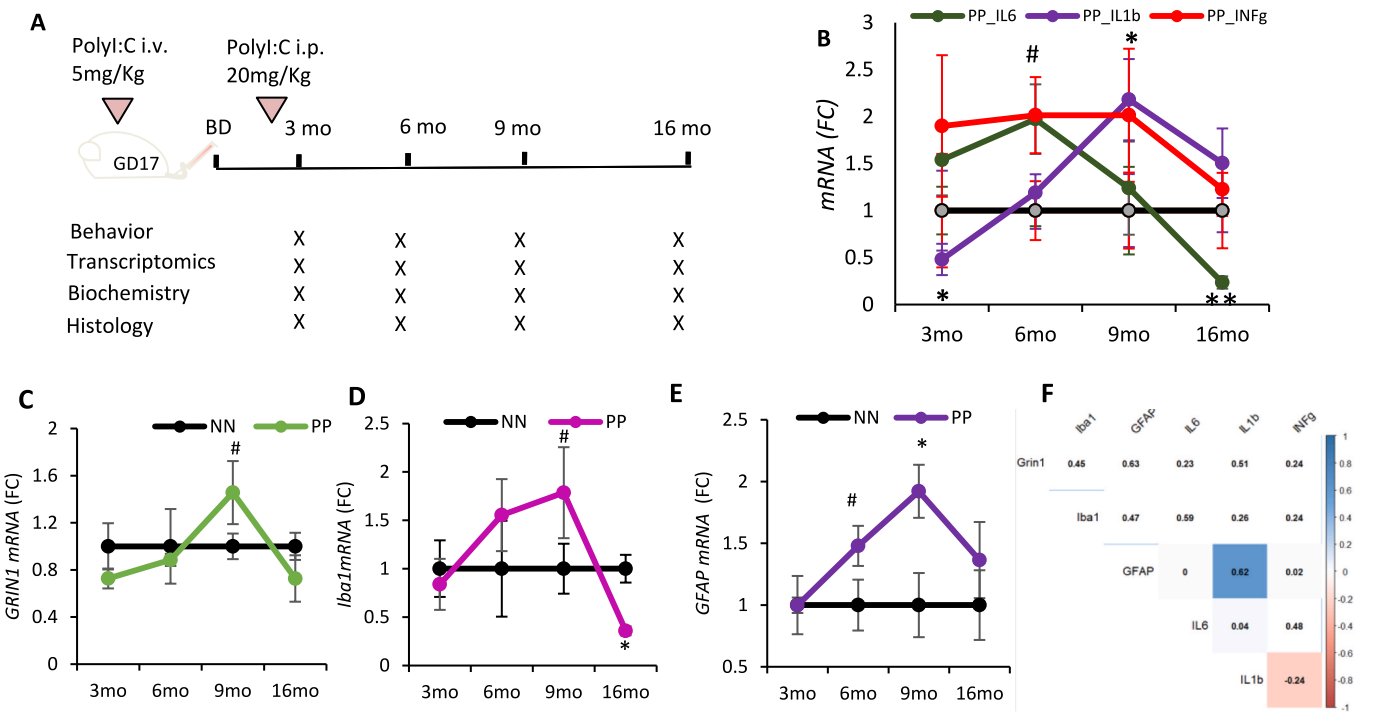

Fig. 1. The neuroinflammatory evolution in aging PolyI:C mice: **(A)** Timeline of the experimental procedure and PolyI:C injections. **(B)** qPCR quantification of pro-inflammatory cytokines (IL-6, IL-1beta, INF-gamma) in the hippocampus after the PolyI:C treatment. Transcript analysis for **(C)** neuronal (GRIN), **(D)** microglia (Iba1) and **(E)** astroglial (GFAP) markers; represented as mean ± SEM, n = 4–5 mice per age and treatment. *p < 0.05, **p < 0.005, #p = 0.07. Statistical significance based on two-way ANOVA with Bonferroni post hoc analysis. **(F)** Correlation matrix indicates the associations between time series of Grin1, Iba1, GFAP with the examined cytokines. Highlighted squares with significant correlation. GD = gestational day, BD = birth day.

with RSeQC version 2.6.4; 4) Get read distribution with RSeQC version 2.6.4; 5) Get gene body coverage with RSeQC version 2.6.4; 6) Get read counts for genes with htseq-count release_0.11.1; 7) perform differential expression analysis with DESEQ2.

Further functional enrichments were performed using the ClueGO (Bindea et al., 2009) which integrates Gene ontology (GO), KEGG (Kyoto Encyclopedia of Genes and Genomes), Wikipathway, and Reactome pathway analysis creating a functional pathway network.

2.12. Reverse transcription-polymerase chain reaction (RT-PCR)

1 μg of total RNA from the human and mouse brain specimen was reverse-transcribed using the M-MLV reverse transcriptase (Promega) for efficient synthesis of the first-strand cDNA. Gene expression analysis was done by RT-PCR (GoTaq qPCR Master Mix, Promega, USA) using gene-specific primers (Suppl. Table 3) on Mic qPCR Cycler (BioMolecular Systems, USA). Expression levels of genes of interest were determined using the ΔΔCT method; the levels of the mRNAs of interest were normalized against the levels of the housekeeping gene, β-actin.

2.13. Antibodies & reagents

The following antibodies were used for Western blot immunolabeling and immunohistochemistry experiments in this study:

Rabbit anti pTau 231 (1:500, ab151559, Abcam, UK), Rabbit anti pTau 205 (1:500, ab181206, Abcam, UK), goat anti-tau (1.25 μg/mL; AF3494, R&D systems, USA), mouse anti-β actin, 1:2000 (sc-81178; Santa Cruz Biotechnology, USA), Rabbit anti GFAP (1:500, ab68428, Abcam, UK), Goat anti GFAP (1:500, SAB2500462, Sigma), Goat anti Iba1 (1:500, ab5076, Abcam, UK), Mouse anti-amyloid-β 6E10 clone [antibody recognizing the amino acid region 1–16 (Aβ1-16); 1:500, cat:803014; Biolegend, USA], S97 Rabbit polyclonal pan-Aβ antibody (1:2500, kindly provided by Dr. Cynthia Lemere), 3A1 Mouse monoclonal anti-Aβ 1–15 (1:1000, kindly provided by Dr. Cynthia Lemere) recognizing β-amyloid but not APP, rabbit anti-synaptophysin (1:500; ab14692, Abcam, UK), Rabbit anti-Lipocalin-2/LCN2 (1:500, 50060-RP02; Sino Biological, China), mouse anti-NF200 (1:500, cat:1178709; Boehringer Mannheim Biochemica, Germany), Biotinylated Lycopersicon Esculentum Lectin (Tomato; Vector Labs, B-1175-1), Nile Red (2 μg/mL, N3013, Sigma, USA).

The secondary antibodies used in the study for immunolabeling were: directly conjugated to Cy2, Cy3, or Cy5 raised in donkey (all 1:1000; Jackson Immuno Europe, UK). DAPI (4′,6-diamidino-2-phenylindole, Cat. no. 10236276001 Roche, Switzerland) was used to visualize nuclear morphology. Biotinylated secondary antibodies were revealed with Alexa Fluor 488 conjugated streptavidin (1:500, Life technologies, 532354).

2.13.1. Western blot

Hippocampal lysates were denatured at 95 °C using the 2-Mercaptoethanol based loading buffer. Proteins were separated using the SDS-polyacrylamide gel electrophoresis and Western blot procedure. Custom-made 8–10% gels were used to run the samples for 1.5 h at 110 voltage. The proteins were then transferred to a precut 0.2 μm nitrocellulose membrane (Cat: 1620146; Biorad, USA) using a wet transfer method (Biorad). Later the membranes were incubated in a blocking solution containing 0.5% bovine serum albumin (Art. No. 8076.4, Roth, Germany), 1xTBS, and 0.1%Tween-20 for 30 min at room temperature on a rotating shaker. The membranes were then incubated with primary

Table 3
Summary of Patients' cohort I.

Stage	N. patients	F: M	Age (mean ± SD)	Braak (mean ± SD)
CTL	9	5: 4	81 ± 8.8	1.0 ± 0.5
MOD	5	3: 2	85 ± 2.2	4.0 ± 1.6
AD	10	4: 6	82 ± 9.9	5.6 ± 0.5

CTL = healthy controls; MOD = moderate AD; AD = severe AD.

antibodies overnight at 4 °C with gentle agitation. On the second day, the membranes were rinsed with TBS-Tween solution 3 × 5 min, followed by a 1-h incubation with the fluorescently conjugated secondary antibodies, rinsed again, and air-dried covered by aluminum foil. The proteins were detected using the Omega Lum (Labgene, CH). The optical density of the protein bands was determined using Image J software and normalized to the Beta-actin control. For an accurate total protein quantification REVERT stain (LI-COR Biosciences-GmbH, Germany) was also employed.

2.14. Fluorescent immunohistochemistry

The mice sagittal tissue sections from the anti-freezing medium were taken and then mounted onto the superfrost glass slides, air-dried for 1 h, and washed twice in distilled water for 5 min each. To access epitopes slides were incubated at 65 °C (water bath) for 20 min in 10 mM Sodium citrate (pH 6) containing 0.05% Tween (Preheat buffer). Thereafter, sections were washed 3 times 5 min each in 1x Trizma-based salt solution (TBS), at room temperature, and once in a TBST buffer (1x TBS containing 0.1% Triton solution). Sections were blocked in the blocking solution (TBST buffer containing 10% fetal bovine serum) for 1 h at room temperature in a humid chamber. Further, the sections were incubated with the primary antibody in the TBST buffer containing 1% fetal bovine serum at 4 °C in the refrigerator overnight. The next day, sections were washed 3 times for 5 min each in the TBS buffer before being incubated with the fluorescently labeled secondary antibodies for 3 h at room temperature. Following the labeling, the sections were washed 3 times in 1x TBS buffer, 5 min each, and mounted with custom-made aqueous mounting media containing 1,4-Diazabicyclo[2.2.2]octane (803456 EMD Millipore, USA). For the lipid droplet Nile red staining, sagittal brain sections were mounted onto the glass slide and air-dried, followed by a rinse with deionized water for 1–2 min. Nile red/glycerol staining solution (2 μg/ml) was added onto the tissue, incubated for 5 min, and coverslipped before being examined using a confocal fluorescence microscope (Zeiss LSM 800, Germany). For blood vessels staining, after blocking with goat serum, tissue sections were incubated overnight with biotinylated lectin and later probed for 3 h with Streptavidin Alexa Fluor 488 conjugate.

2.15. Image quantification

To quantify the glial response to an increase in systemic and central inflammatory profile, the morphology of these brain innate immune cells has been analyzed. Iba-1 positive microglia images (10 ROI/section) were taken at 40x oil immersion objective using a Confocal microscope (Zeiss LSM 800, Germany) with 1 μm Z intervals resulting in stacks of 20–30 slices at 512 × 512-pixel resolution. The soma area, perimeter, circularity, skeleton analysis was performed as instructed (Young and Morrison 2018; Davis et al., 2017) and using custom-made macros (Suppl. Materials and Methods). For the Fractal analysis on aged mice microglia 60x Oil immersion objective was used to generate in-depth microglia morphological data. Mean fluorescence intensity (pTauT231) of the CA1 field was measured in the same age group using the ImageJ ROI manager. Lcn2 staining was analyzed for % area coverage using the custom-made ImageJ macros (Suppl. Materials and Methods). Nile red positive lipid droplets were analyzed using the Analyze particle function in ImageJ. For the histological data, ImageJ macros were created and used for the analysis for an unbiased morphological quantification (Suppl. Materials and Methods).

2.16. Statistical analysis

Homogeneity of variance for each variable within a group age was verified by Levene's Test Statistical significance was assessed using unpaired, 2-tailed Student's t-test and ANOVAs followed by either Bonferroni or Benjamini Krieger and Yekutieli or Fisher LSD as specified in the figure legends. Results (mean ± SEM) were obtained using GraphPad Prism 8. *P* values less than 0.05 were considered significant. RNA sequencing data were analyzed using the `R`DESEQ2 package and statistically significant transcripts were chosen if $p < 0.05$ and p adjusted for multiple testing <0.1. For the flow cytometry data, statistical analysis was performed through unpaired Welch's *t*-test using GraphPad Prism Version 8.1.2. Optical densities of immunoblots were compared between groups using ANOVA with Post-hoc Bonferroni correction. Morphology measurements of microglia were analyzed using the Kolmogorov–Smirnov test and in aggregate using ANOVA. Correlation analysis was conducted using R and significance tested using Student's t-test.

3. Results

3.1. Chronic inflammation after double PolyI:C challenge

Double-challenged PolyI:C animals were injected in prenatal life at gestational day 17 and in the offspring at 2.5 months (PP). Animals were analyzed cross-sectionally at 3, 6, 9, and 16 months, taking saline-injected controls as reference (NN) (Fig. 1A). From 3 to 6 months of age levels of four circulating inflammatory cytokines (MCP-1, IL-6, TNF-α, and IL-10) are progressively higher in PP as compared to NN (Table 1). A two-way ANOVA highlights that the observed differences in the TNF α levels between treatment are due to the effect of age ($F_{3,37} = 95$, $p < 0.001$) based on the interactions between age and treatment ($F_{3,37} = 3$, $p < 0.05$), with higher levels in the 6 months PP mice than the other ages ($F_{1,14} = 9.4$, $p < 0.005$). We also observed a significant effect on IL-6 expression after PolyI:C treatment with aging ($F_{3,37} = 17$, $p < 0.001$) based on the interaction between treatment and age ($F_{3,37} = 17.59$, $p < 0.00005$) with a peak of plasma IL-6 levels in 9 months PP mice ($F_{1,8} = 71$, $p < 0.00005$). Later at 16 months, NN and PP mice show no difference in humoral immune factors (Table 1). Considering the upregulation of a large population of circulating chemokines in the blood of PP mice from 3 months of age, we examined the neutrophils, monocytes, and total polymorphonuclear cells (PMNs) from the freshly isolated whole blood and brain samples to study any infiltration of these leukocytes into the brain. Samples were analyzed using the flow cytometry for the expression of neutrophils and monocytes using antibodies stained for Ly6G, Siglec, F4/80, CD11b. Although no changes are observed at 3 months of age between groups, at 6 months PP mice exhibit elevated levels of neutrophils and PMNs in the systemic circulation but no significant differences are seen in the brain of PP mice as compared to NN animals (Suppl. Fig. 1A and B). On the other hand, the monocyte population differs neither in the blood nor in the brain (Suppl. Fig. 1C).

While there is no trace of infiltrating immune cells in the brain at 3 or 6 months, analysis by RT-PCR of *IL-6* transcripts shows a significantly different trend between PP and NN mice over time with aging ($F_{3,30} = 4.4$, $p < 0.05$) based on the interaction of treatment with age ($F_{3,30} = 10.9$, $p < 0.005$). After a peak at 6 months ($F_{1,8} = 1.5$; $p = 0.05$), *IL-6* decreases significantly in the brain of PP mice compared to saline controls ($F_{1,8} = 5.25$, $p < 0.005$; Fig. 1B). Further, *IL-1β* expression in PP brains changes over time with aging ($F_{3,30} = 4.24$, $p < 0.05$), starting from lower levels in PP brains at 3 months ($F_{1,8} = 6.44$, $p < 0.01$) followed by a peak at 9 months ($F_{1,8} = 3.4$, $p < 0.05$; Fig. 1B). The effect of treatment on the expression of Interferon-gamma (IFNγ), a cytokine critical against viral infections, showed a significant effect between the groups ($F_{1,30} = 4.7$, $p < 0.05$) and a slight difference over time ($F_{3,30} = 2.49$, $p < 0.07$) with a rise in expression of IFNγ in PP brains at 6 months as compared to NN ($F_{1,10} = 6.78$, $p < 0.05$; Fig. 1B).

We further analyzed how the inflammatory transcripts correlate with cell-type-specific transcripts for neurons (*GRIN1,* Glutamate Ionotropic Receptor NMDA Type Subunit 1), microglia (*Iba1;* Ionized calcium-binding adaptor molecule 1), and astroglia (*GFAP;* Glial Acidic Fibrillary Protein) in PP and NN animals. We observe that *GRIN1* expression is

stable except for a trending increase at 9 months (Fig. 1C), whereas *Iba1* shows dynamic changes with a progressive increase from 6 to 9 months and a drop at 16 months ($F_{1,8} = 5.9$, $p < 0.05$) (Fig. 1D) similarly to the proinflammatory cytokines (*IL-6*, r16mo = 0.77, and *IL-1β*, r16mo = 0.68). At 6 months ($F_{1,8} = 1.7$, $p = 0.19$) and 9 months ($F_{1,8} = 7.5$, $p < 0.05$), *GFAP* expression increases but decays to normal levels at 16 months (Fig. 1E). The temporal evolution of *GFAP* overlaps with that of IL-1β, (rt = 0.62, $p < 0.05$; Fig. 1F). Our results show that the combination of prenatal and an early postnatal PolyI:C immune activation causes a prolonged and sustained systemic inflammatory response with the recruitment of circulating leukocytes of the innate immunity, increased neuroinflammation, and glial gene expression at mid-age.

3.2. Progressive tauopathy in PP mice

We determined the impact of systemic immune challenge on the pretangle pathology by analyzing tau hyperphosphorylation at positions 231 and 205 using Western blot (Fig. 2A) and immunohistochemistry (Fig. 2F and Suppl. Fig. 2A) on hippocampal tissue from 3 to 16 months of age. The content of hippocampal p-tau (pTau T231) relative to total tau (ptau/tau) indicated significant effect of treatment between PP and NN ($F_{1,30} = 11.5$, $p < 0.005$), aging ($F_{3,30} = 6.7$, $p < 0.005$) and significant interaction between treatment and age ($F_{3,30} = 5.6$, $p < 0.005$). Specifically, ptau/tau increases dramatically in PP mice at 6 months, ($F_{1,7} = 21.7$, $p < 0.00005$), remains elevated at 9 months ($F_{1,8} = 10.5$, $p < 0.005$), and then is indistinguishable from NN mice at 16 months (Fig. 2B and C). The progressive tauopathy is confirmed by immunolabeling of pTau fibers (pTau T205) in the hippocampal CA1 region and CA1 stratum lacunosum (Suppl. Fig. 2A), with a significant increase in pTau pixels in the CA1 region at 16 months (Suppl. Fig. 2B). Tau hyperphosphorylation can be observed in the CA3 field at 9 months in PP mice, in contrast to NN (Fig. 2F). To assess whether the progressive tauopathy in PP is associated with synaptic abnormalities and neuroinflammatory responses, we quantified the levels of synaptophysin and GFAP over time (Fig. 2D). At 16 months in PP mice, we observe a non-significant drop in synaptophysin expression accompanied by a significant increase in GFAP ($F_{1,30} = 10.04$, $p < 0.005$) (Fig. 2E). The increase in GFAP immunoreactivity is confirmed by immunohistochemistry of the CA3 region showing the presence of amyloid-β1-16 and small p-tau aggregates (Fig. 2G; insert). Further, we saw in the 16 months old mice the internalization of amyloid-β1-16 in GFAP positive glial cells, which is more pronounced in PP mice (Fig. 3A, white stars). Due to the cross-

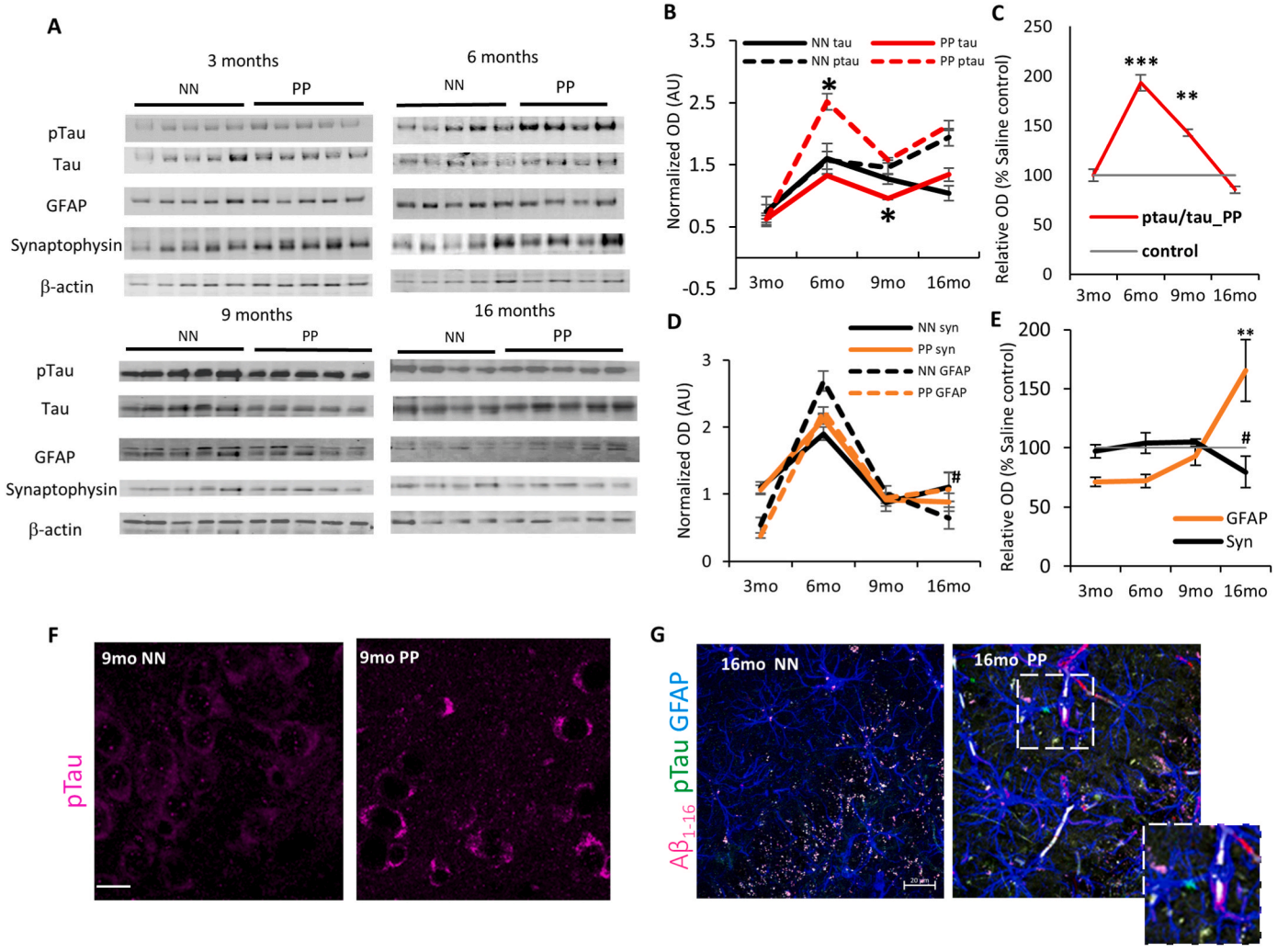

Fig. 2. The Effect of PolyI:C on p-tau accumulation in the hippocampus: (A) Immunoblots of hippocampal lysate from PP and NN mice at 3, 6, 9 and 16 months, for p-tau, tau, GFAP, Synaptophysin. β-Actin was used as housekeeping control. **(B,D)** Relative quantification of Tau, GFAP and Synaptophysin represented in normalized optical density. **(C,E)** Percentage of relative changes of these proteins compared to the saline treated controls. Representative immunostaining for **(F)** p-tau (9 months) and **(G)** p-tau, $A\beta_{1\text{-}16}$ and GFAP at 16 months age group. Insert shows a GFAP positive process with internalized p-tau aggregates. Scale bar in F is 45 μm, G is 20 μm. Values represented as mean ± SEM, n = 4–5 mice per age and treatment. *$p < 0.05$, **$p < 0.005$, ***$p < 0.0005$ #$p = 0.07$. Statistical significance based on two-way ANOVA with Bonferroni post hoc analysis.

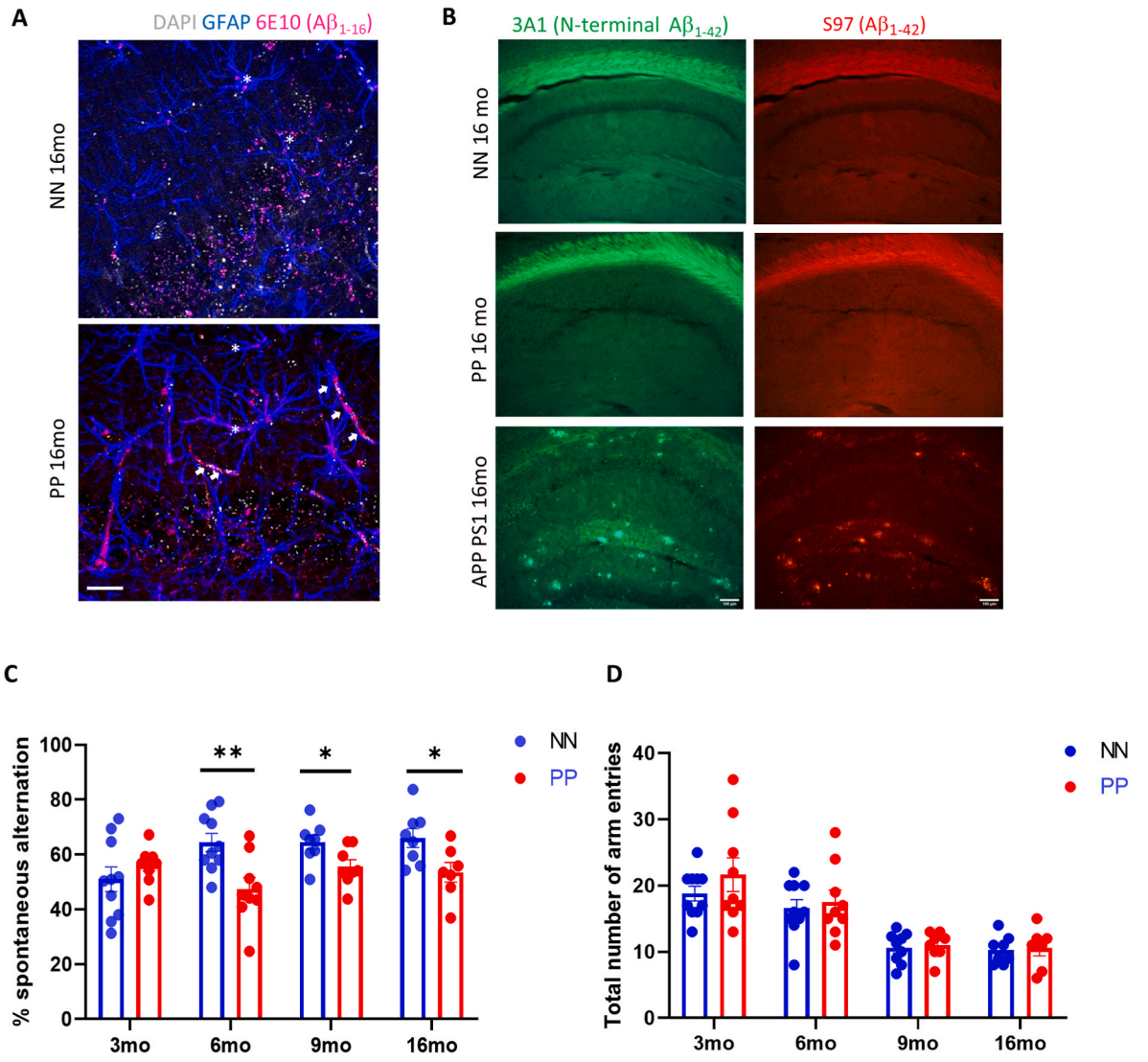

Fig. 3. Amyloid immunostaining in the hippocampus and spatial memory deficits. **(A)** Double immunolabeling for $A\beta_{1\text{-}16}$ and GFAP shows internalization of amyloid in GFAP + glia cells (stars) in NN and PP mice at 16 months and depositions of amyloid in vessels (white arrows) in PP mice. **(B)** Representative immunostaining of S97 and 3A1 anti-β-Amyloid antibodies in the hippocampus of aged 16 months PP, NN controls and APP PS1 positive control, showing no signs of plaque formation after PolyI:C treatment **(C)** Effect of PolyI:C treatment on memory task assessed with Spontaneous alternation indicate a significant impairment in the percent of spontaneous alternation entry in PP mice compared from 6 to 16 months as compared to NN (n = 7–10 mice per treatment and age). **(D)** Regardless of treatment, 9mo and 16mo old mice showed less total number of arm entries. Values in bar charts and line graph are represented as mean ± SEM. *p < 0.05, **p < 0.005, two-way ANOVA followed by Benjamini Krieger and Yekutieli post hoc analyses. Scale bar in A = 20 μm and B = 10 μm. Abbreviations: NN = prenatal & postnatal saline injected controls, PP = prenatal and postnatal PolyI:C treated mice.

reactivity of Aβ antibodies (like clone 6E10) with amyloid precursor protein (APP), we further analyzed amyloid pathology in these mice using a pan-Aβ antibody (S97) and an N-terminal specific Aβ antibody (3A1) that does not recognize APP. Our immunohistochemical data showed no signs of amyloid aggregation or plaque formation when tested with both the Aβ antibodies while confirming with a positive control slide tissue from APP PS1 mice (Fig. 3B).

3.3. PolyI:C induced memory impairment

Based on the increased tauopathy in the hippocampal region following double PolyI:C injection, we assessed whether spatial working memory is affected. Previous work has shown that spontaneous alternation, a form of working memory, is entirely dependent on hippocampal synaptic function (Pioli et al., 2014; McHugh et al., 2008). The same set of PP and NN animals were subjected to the Y-maze spontaneous alternation task at 3, 6, 9, and 16 months. The percentage spontaneous alternation (Fig. 3C) and the number of arm entries (Fig. 3D) were recorded and calculated. There was a significant effect of age on the percentage of spontaneous alternation ($F_{1,61} = 11.32$, $p = 0.0013$). Post hoc analysis revealed significant deficits in spontaneous alternation in the PP group both *at* 6 months ($p = 0.005$), 9 months ($p = 0.02$) and 16 months ($p = 0.02$). The number of arm entries in the Y maze task is not significantly different between the treatments at each age group (Fig. 3D) indicating normal locomotory behavior reflecting a non-confounding factor for the percentage of an alteration. However, regardless of the treatment, from 9 months of age both PP and NN display about half of the number of entries as compared to younger animals. Since early and late gestational PolyI:C treatment has been linked to stress and anxiety-like phenotypes relevant to schizophrenia (Hui et al., 2018; Silveira et al., 2017) we tested these mice for Light/-dark, Elevated O-maze at 3 and 6 months, and Open field tasks at all ages. We found no difference in the anxiety-like behavior (Suppl. Table 4) disambiguating the spatial memory impairments observed.

Table 4
Summary of Patients' cohort II.

Stage	N. patients	F: M	Age (mean ± SD)	Braak (mean ± SD)
CTL	5	2: 3	80 ± 5.9	2.3 ± 0.5
VaD	6	3: 3	82 ± 3.5	4.0 ± 1.6

CTL = healthy controls; VaD = Vascular dementia.

Together the data suggest that prenatal and early postnatal viral-like immune activation through PolyI:C treatment causes tauopathy of the limbic regions with sustained working memory impairment.

3.4. Activation and phenotypic change in microglia of PP animals

Earlier studies have shown that systemic infections and the subsequent peripheral immune activation have a strong effect on brain function, glial response represents a risk for dementia (Cunningham and Hennessy 2015; Cunningham 2013). Microglia cells are the primary phagocytic innate immune cells of the brain that get stimulated upon immune activation. They normally exist in a resting state displaying a ramified morphology, while intermediate states display a bipolar or rod-like phenotype (Davis et al., 2017) and in an activated state an amoeboid, irregular shape (Ling and Wong 1993). Quantification of Iba-1 positive cells per mm^3 in the immunostained hippocampus (Fig. 4A), indicates no difference between PP and NN at the different stages (Suppl. Table 5). Next, we assessed whether the PP brains show altered microglial cell morphologies reflecting an activated inflammatory status. We quantified morphological parameters like soma size, perimeter, circularity, skeleton analysis of Iba-1 positive microglia (Fig. 4), and finally we conducted the fractal analysis in NN & PP mice across staging. Quantitative soma analysis shows a significant increase in the soma size, typical of activated microglia in PP mice at 9 months ($p < 0.05$) and a non-significant increase at 16 months (Fig. 4B), while no changes were detected in microglial soma perimeter size across stages (Fig. 4B). The circularity of the soma, indicating the roundness index, showed no changes in PP mice compared to saline controls across the stages (Fig. 4B). These changes were further analyzed using the distribution curve analysis which indicates an overall shift in the number of cells with an increase in microglial cells soma size and perimeter (Suppl. Fig. 3A and 3B) with irregularly shaped cell bodies during the adult, mid-aged intermediate stages and in aged mice (6,9 and 16 months)), suggesting morphological fluctuations across staging and signs of microglial activation (Suppl. Fig. 3C). To further characterize the phenotypic changes in microglia, reflecting their activation state, we performed the skeletal analysis of Iba-1 positive microglia, at 3, 6, 9, and 16 months in PP and NN mice. Skeletonized Iba-1 renderings reveal an increasing trend in the number of endpoints/cell in the PP mice until 9 months and a significant drop at 16 months. In terms of microglial maximum branch length, we observed the effect of treatment with reduction in branch length only in the aged 16 months PP mice ($p < 0.05$) (Fig. 4C). Interestingly, these microglia that showed a decreasing trend in their soma roundness in the aged 16 months PP mice, have retracted process lengths as measured by a significant drop in their maximum branch length indicating morphological signs of activation as observed in other inflammation models (Tejera et al., 2019). . Prenatal and early postnatal systemic PolyI:C immune activation induces dynamic changes in microglial phenotype in early-mid aged mice, however, in the later life microglia undergo bushier with the reduction in microglial end-points and branch lengths.

Having detected a microglia morphological transition in aged 16 months PP mice, confocal imaged microglia cells were further investigated using fractal analysis (FracLac plugin of ImageJ) which renders the shape of microglia cells and quantifies the parameters of cell area, cell perimeter, Span ratio, circularity, and fractal dimension, the latter reflecting pattern complexity. The fractal analysis revealed significant changes in hippocampal microglia parameters in the aged 16 months PP mice versus NN (Fig. 4D). Normal resting microglia are complex with a higher fractal dimension. In the PP mice total microglia cell surface area ($t_{(80)} = 43.65$, $p < 0.005$) and the perimeter ($t_{(75)} = 4.2$, $p < 0.005$) is reduced indicating a more compact shape (Fig. 4E and F). Fractal dimension as a measure for complexity and circularity as a measure for the roundness is also reduced ($t_{(62)} = 4.9$, $p < 0.005$) after immune activation (Fig. 4H and I). On the other hand, the span ratio is increased ($t_{(79)} = 1.9$, $p = 0.06$) reflecting microglia elongation (ratio of cell length and width) (Fig. 4G). Span ratio and circularity are inversely proportional indicating an activated microglia state. Altogether, systemic inflammation through pre-and post-natal PolyI:C induces profound changes in microglia morphology indicating a dynamic shift in aged PP animals when compared to earlier age groups.

3.5. Dynamic remodeling of the hippocampal transcriptome

To understand the mechanisms underlying the spatial memory deficits and the pathophysiological processes associated with the proteinopathy, and neuroinflammation we performed a cross-sectional hippocampal bulk mRNA sequencing on 3, 6, 9, and 16 months PP and NN animals. The analysis reveals many differentially expressed genes (DEGs) in the hippocampus (log2 fold change cut-off:05, adjusted $p < 0.05$) between treatments. The gene expression profiles as visualized in the volcano plot (Fig. 5A–D), show that in aged animals differential expression is highest with a peak at 9 months, coinciding with the neuroinflammatory switch in microglia cells. A GO analysis contextualized to the synapse (SYNGO) (Koopmans et al., 2019) indicates a dynamic shift in DEGs from the presynaptic compartment at 3 months (Supp. Fig 4A) to the postsynaptic terminal at 9 and 16 months (Supp. Fig. 4C and 4D), with a non-synaptic stage at 6 months (Supp. Fig 4B). At 3 months, out of 35 DEGs between PP and NN, 21 are downregulated, and 14 are upregulated (Fig. 5A). Gene ontology enrichment analysis (GEA) of the biological processes using a 5% false discovery rate indicates general repression in genes associated with synaptic transmission, calcium signaling, extracellular matrix organization, and secretion (Suppl. Table 6). Pathway analysis based on a composite KEGG, Reactome, WikiPathways dataset shows high interconnectivity between cellular cascades associated with extracellular matrix organization, chemical synaptic transmission, and calcium signaling (Suppl. Fig 5A). In the 6 months, out of 32 DEGs between PP and NN (Fig. 5B), 22 are downregulated, and 10 are upregulated. A GEA indicates ongoing processes of morphogenesis and gliogenesis (Suppl. Table 6), with highly overlapping pathways (Suppl. Fig. 5B). At 9 months (Fig. 5C) out of 196 DEGs, 90 are downregulated, and 106 are upregulated. The GEA shows enrichment in several processes associated with vascular remodeling, neurogenesis, morphogenesis, cytokine response, and cell death (Suppl. Table 6). Pathway analysis indicates partially overlapping cellular cascades shared among focal adhesion, BMP signaling, MAPK signaling, and neuronal injury (Suppl. Fig. 5D) confirming the concurrent processes of morphogenesis and cell death at this stage. In the 16 months PP mice (Fig. 5D) from the 99 DEGs, 50 genes are downregulated and 49 genes are upregulated. GEA of the DEGs indicates enrichment in the response to metal ions, the reactive oxygen response, morphogenesis, the regulation of cellular proliferation, and the response to hormones (Suppl. Table 6). Pathways analysis shows less interconnected cascades implicated in potassium ion transmembrane transport, monocytes proliferation, lamellipodium organization, and glucose metabolism (Suppl. Fig. 5D).

To better understand the dynamic changes in the sterile infection model undergoing with age, we compared the significantly differentiated genes between PP and NN at the cross-sectional time points. As shown in the Venn diagram (Fig. 5E), the number of common genes that are uniquely and commonly affected in the hippocampus of 3, 6, 9, 16 months PP mice indicates a large number of overlapping gene sets between 9 and 16 months, while fewer genes are shared with earlier stages. In particular, 6 shared genes can be subdivided into 2 categories

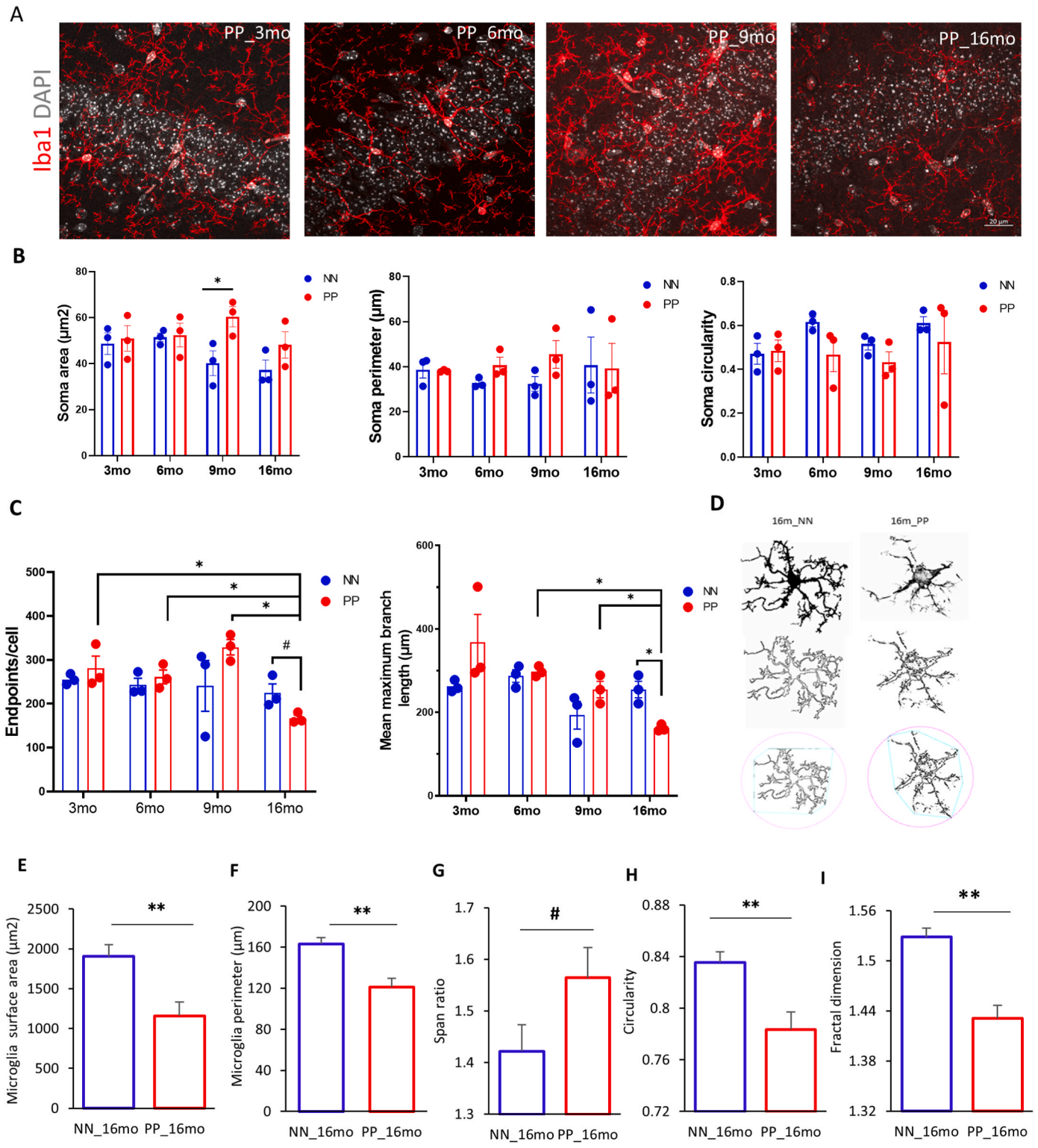

Fig. 4. Longitudinal changes in hippocampal microglia: **(A)** Immunofluorescence staining for Iba1 staining in the PolyI:C treated mice. **(B)** Dynamic changes in microglia soma size, perimeter and circularity were quantified in Saline(NN) and PolyI:C (PP) mice in different age groups. (n = 3–4 mice per group & condition, data points come from 4 equidistant planes and at least 5 ROI`s/animal,*p < 0.05, two-way anova followed by Fisher's LSD test) **(C)** Bar chart representing the effect of treatment and aging on the average endpoints maximum branch length per cell (n = 3 mice per age group and condition, *p < 0.05, two-way ANOVA, followed by Benjamini Krieger and Yekutieli post hoc analyses, #p = 0.09) **(D)** Example of fractal analysis of microglia from the hippocampus of PolyI:C and saline treated 16 months aged mice. 63x single cell fractal analysis indicate the surface area **(E)** and perimeter **(F)** were decreased in PP mice, in contrast to the span ratio **(G)** showed a higher trend. PP mice showed a significant decrease in cell circularity **(H)** and fractal dimension **(I)**, n = 45 cells from 3 mice per group and condition, mean ± SEM. #p = 0.07,*p < 0.05, **p < 0.005 Student's t-test. Scale bar, A = 20 µm.

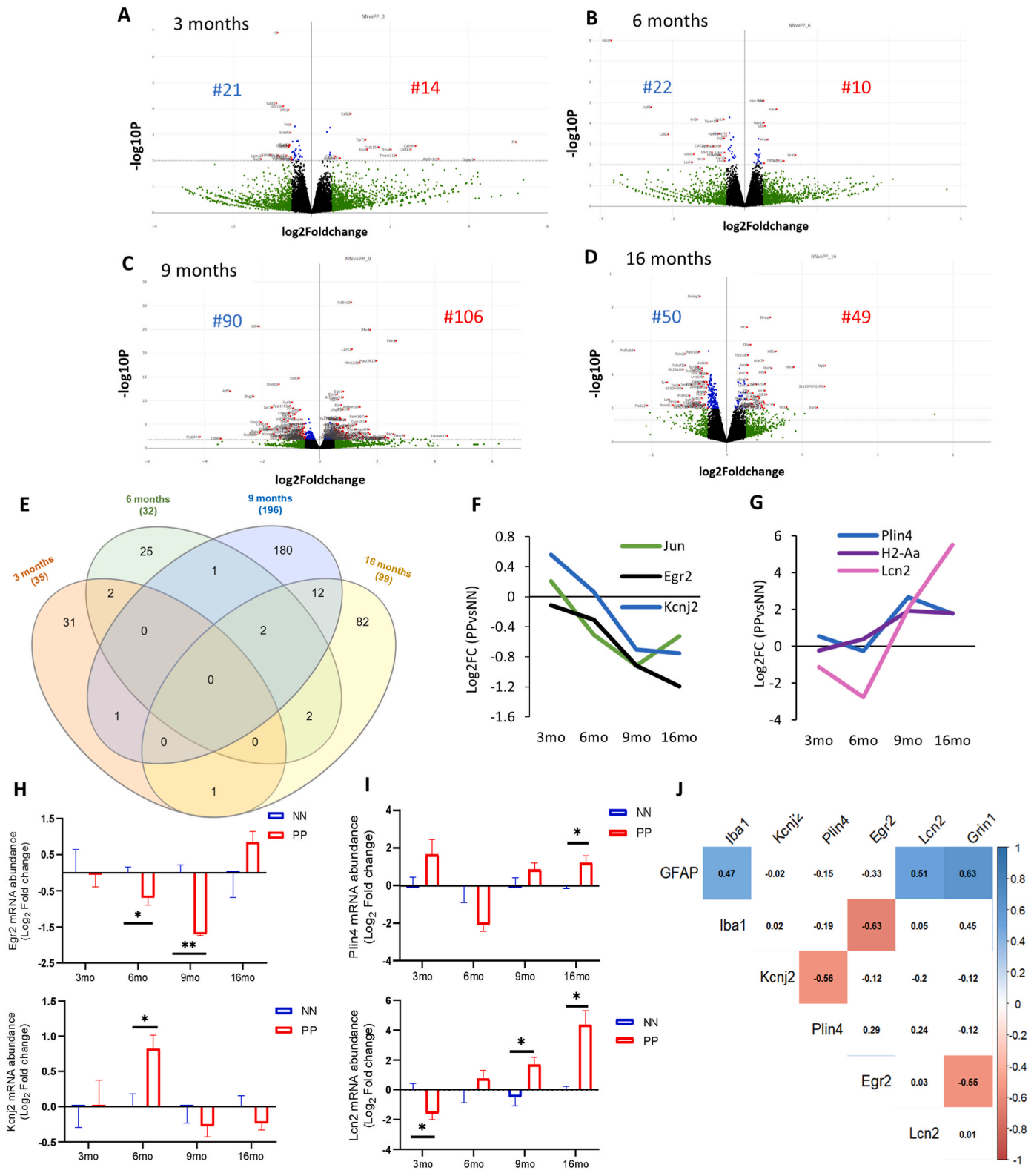

Fig. 5. Bulk transcriptomics analysis of hippocampus in the aging PolyI:C. Gene expression changes after the prenatal and early postnatal immune challenge. Volcano plot with log2-fold change (X-axis) and -log10 p-value (Y-axis) at different age groups **(A)** 3 months **(B)** 6months **(C)** 9 months and **(D)** 16 months in PP versus NN controls. Genes with log2 fold changes >0.5 are shown in green. Significantly regulated genes are shown in red (log2 fold change >0.5, $p < 0.05$, left downregulated and right upregulated). Genes with insignificant log2 fold changes <0.5 are shown in black [controls (NN) n = 3/age, PolyI:C (PP) n = 3/age. **(E)** Venn diagram indicating the number of uniquely and commonly affected genes in the aging hippocampus following prenatal and early postnatal PolyI:C (PP) treatment. Few common genes along with their Log2 Fold changes either **(F)** downregulated or **(G)** upregulated were plotted across staging. Transcript validation analysis for **(H)** *Egr2* and *Kcnj2* and **(I)** *Plin4* and *Lcn2*, $*p<0.05$, $**p<0.005$, two-way ANOVA with Benjamini Krieger and Yekutieli post hoc analyses, [controls (NN), n = 5/age, PolyI:C (PP) n = 4–5/age] **(J)** Spearman correlation matrix for mRNA levels (Log_2FC) with highlighted significant association from 9 to 16 months among the differentially expressed cell-type markers (*GFAP, Iba1* and *Grin1*) and *Egr2, Kcnj2*, *Plin4* and *Lcn2* between PolyI:C and saline.

reflecting a progressive cell-communication dysfunction (I) and a proinflammatory drive (II) in aging PP mice. (I) Genes downstream of MAPK-signaling (*c-Jun*) (E. K. Kim and Choi 2010), NFKB-signaling (*Egr2;* Early growth response protein 2) (Williams et al., 1995), responsible for neuronal excitability (*Kcnj2;* Potassium Inwardly Rectifying Channel Subfamily J Member 2) (Binda et al., 2018), with reported association with synaptic dysfunction, are downregulated in PP mice starting from 6 months (Fig. 5F). (II) On the other hand, genes related to neuroinflammation such as the lipid-droplet dependent gene (*Plin4;* Perilipin 4) (Han et al., 2018), pro-inflammatory genes (*H2-Aa*; Immunohistocompatibility-complex) (Van Hove et al., 2019), and acute-phase proteins regulating to the inflammatory response (*Lcn2*; Lipocalin-2) (Dekens et al., 2020) are upregulated in aging PP mice, starting from 9 months (Fig. 5G). Overall, the gene remodeling across the aging continuum replicates processes typical of a neuronal network breakdown, altered immune response, chronic neuroinflammation, and vascular dysfunction.

3.6. Substantial changes in brain metabolism and inflammation

We further validated the RNA-seq analysis via RT-PCR, on some of the significant DEGs with a reported association to neurodegeneration, vascular changes. Longitudinal transcriptomic changes for some genes with dynamic changes across aging and belonging to the neuronal; Egr2 and Kcnj2 (Fig. 5H) and metabolic Plin4 and Lcn2 (Fig. 5I) gene groups were analyzed separately. RT-PCR validation for some genes with significant changes at specific ages was also analyzed (Table 2). At 3 months, *Cacna1g* (Calcium Voltage-Gated Channel Subunit Alpha1 G), which was previously reported to decay with aging and regulate amyloid-β production (Rice et al., 2014), is unchanged (Table 2; $p = 0.77$) in contrast to the observed reduction via RNA-seq (Log2FC = −0.6), suggesting that aggregate changes rather than single-gene changes may contribute to the modeled conductivity dysfunction (Suppl. Table 6). As expected at this stage, *Plin4* and *Egr2* are unchanged, matching the RNAseq data (Table 2). At 6 months, we analyzed one of the genes associated with cognitive impairment in chronic cerebral hypoperfusion (Xie et al., 2018), the *Glpr2* (Glucagon-Like Peptide 2 Receptor), is strongly downregulated at the RNA-seq and an 80% decrease in RT-PCR analysis (Table 2; $p < 0.05$). Also, *Ide* (Insulin-degrading enzyme), which has been implicated in the clearance of insulin (Qiu and Folstein 2006), shows a comparable increase, between RNA-seq and RT-PCR analysis, but did not reach significance in the RT-PCR result (Table 2; $p = 0.16$). Interestingly, *Kcnj2* shows a significant 2 fold increase at 6 months (Table 2; $p < 0.05$), suggesting a modulatory K^+ currents effect and *Egr2* shows a significant decrease ($p < 0.05$). *Plin4* remains unchanged between PP and NN at 6 months in both analyses (Table 2). At 9 months, the reduction in *c-Jun* ($p < 0.05$), *c-fos* ($p < 0.05$), *Notch1* ($p < 0.005$), *Egr2* ($p < 0.05$), and the increase in *Lcn2* ($p < 0.05$) can be confirmed at the RT-PCR, while *Plin4* show a non-significant increase usfing RT-PCR (Table 2; $p = 0.24$). At 16 months, *Lcn2, Plin4* ($p < 0.05$) trends are reproduced according to the RT-PCR, while *Kcnj2* shows a comparable but not significant decrease (Table 2; $p = 0.36$). The data indicates that around ¾ of the RNA-seq outputs could be replicated via RT-PCR validation, confirming the robustness of the bulk RNAseq discovery method and emphasizing that aggregate dataset can explain ongoing cellular and molecular processes in such models. Validated DEG profiles of *Kcnj2*, *Egr2,* and *Plin4* and *Lcn2* are matched with the expression of genes specific for neurons (*Grin1*), microglia (*Iba1*), and astroglia (*GFAP*) with age continuum in PP mice to investigate associations of the selected genes in specific cell types (Fig. 5J). In the treatment group with aging, *GFAP* expression was positively correlated with *Lcn2*, *Grin1*, *Iba1* expression as also seen evident in RT-PCR data (Fig. 1C–E) supporting the neuro-glia interplay. On the other hand, *Egr2* was negatively correlated to Iba1 and Grin1, while Kcnj2 with Plin4. Based on downregulation of *Glpr2* in adulthood, indicating vascular hyperperfusion (Xie et al., 2018) and the subsequent upregulation of the vascular and inflammatory markers, *Lcn-2*, at 9 months, we investigated vascular integrity by validating the gene expression of Kruppel-like factor 4, *Klf-4*, at 9 and 16 months and observed a transient downregulation at 9 months (Table 2). At the same time point, angiogenesis markers such as Cytochrome P450 Family 1 Subfamily B Member 1, *Cyp1b1,* and Angiopoietin-like 4, Angptl4, with reported function in vascular homeostasis and alteration in neurodegenerative disorders like AD (Chakraborty et al., 2018; Ghosh et al., 2016) showed a peak at 9 months, supporting pathological vascular processes in aged adult PP mice. Systemic inflammation and tau accumulation could impact blood vessel integrity and perturb vascularization and vascular density (Bennett et al., 2018; Tremblay et al., 2013) . With changes in vascular related gene expression markers, we also found in the hippocampus of many 16 months PP mice changes in brain microvasculature, and increased vessel density evidenced by lectin staining (Suppl. Fig. 6).

Nevertheless, an increase in Lcn2 has been reported in both AD brains (Dekens et al., 2018; Naudé et al., 2012) and CSF from vascular dementia patients (Llorens et al., 2020a). In line with our PolyI:C model of sterile infection, the increase in Lcn-2 is likely attributed to the production and release by activated microglia, reactive astrocytes, neurons, and endothelial cells in response to inflammatory and infectious insults (Jha et al., 2015). Our immunofluorescence analysis using an antibody specific for Lcn2 shows an increase in Lcn2 protein expression in the hippocampal CA3 field of the PolyI:C mice at 9 months and 16 months aged mice (Fig. 6A). Quantitative analysis of the Lcn2 signal shows a significant increase in the % of the Lcn2 stained area in PP mice in both age groups ($p < 0.05$) (Fig. 6B). To study lipid metabolism and intracellular lipid droplets accumulation, as a sign of neuroinflammation with aging, we have utilized the dye Nile Red which accumulates in lipids and emits red fluorescence (Greenspan et al. 1985). We observed more Nile Red-positive lipid droplets (LDs) in the hippocampal CA3 field with aging, which is even more evident in PP mice as compared to saline controls (Fig. 6C). Triple labeling with Nile Red, Neurofilament L-200, and Iba1, shows that both NF200 positive neurons and Iba1 positive microglial cells have increased lipid droplets (Fig. 6D). Quantitative analysis of the LDs between the PP and NN at the different time points indicates that the density of the LDs is greater in PP mice starting from 6 months ($p < 0.005$) until 9 months ($p < 0.05$), resulting in increased stained area, peaking at 6 months ($p < 0.05$) and 9 months ($p < 0.005$) (Fig. 6E). On the other hand, LDs' size remains unchanged between conditions (Fig. 6E). Although insignificant, there is always an increasing trend of Nile red LDs density and % Nile red-stained area in the aged 16 months PP mice. The histo-anatomical analysis confirms the presence of neuroinflammatory markers that contribute to a neurodegenerative-like neuropathological progression.

3.7. Translation to Alzheimer's disease

To assess whether the newly designed PolyI:C model is reproducing genetic changes in human AD, we performed targeted fingerprinting focusing on a cross-sectional cohort of post-mortem entorhinal cortices containing the hippocampus from age-matched subjects with mild-moderate AD, severe AD, and age-matched healthy controls (CTL) (Table 3 and Suppl. Table 1). We first examined cell-type-specific genes, *GFAP*, *Iba1,* and *MAP2*. Consistently, with our model we observe a progressive increase in *GFAP* expression from Moderate to Severe AD ($F_{2,21} = 9.29$ $p = 0.012$; Fig. 7A and Suppl. Table 7), while *Iba1* and *MAP2* remain unchanged (Fig. 7A and Suppl. Table 7). Next, we examined some of the relevant DEG with reported association with AD and divided them into functional categories. *Glpr2* and *Ide* belonging to the glucose metabolism with differential expression in a 6-month-old PP adult did not show any significant difference between the clinical groups and controls (Fig. 7A and Suppl. Table 7). We next examined *Kcnj2* and *Egr2* which show downregulation in the PP model at 9 months (Table 2 and Fig. 5H) observed high variability with no changes across stages in the clinical AD cohort (Suppl. Table 7 and Fig. 7C). Among the cellular

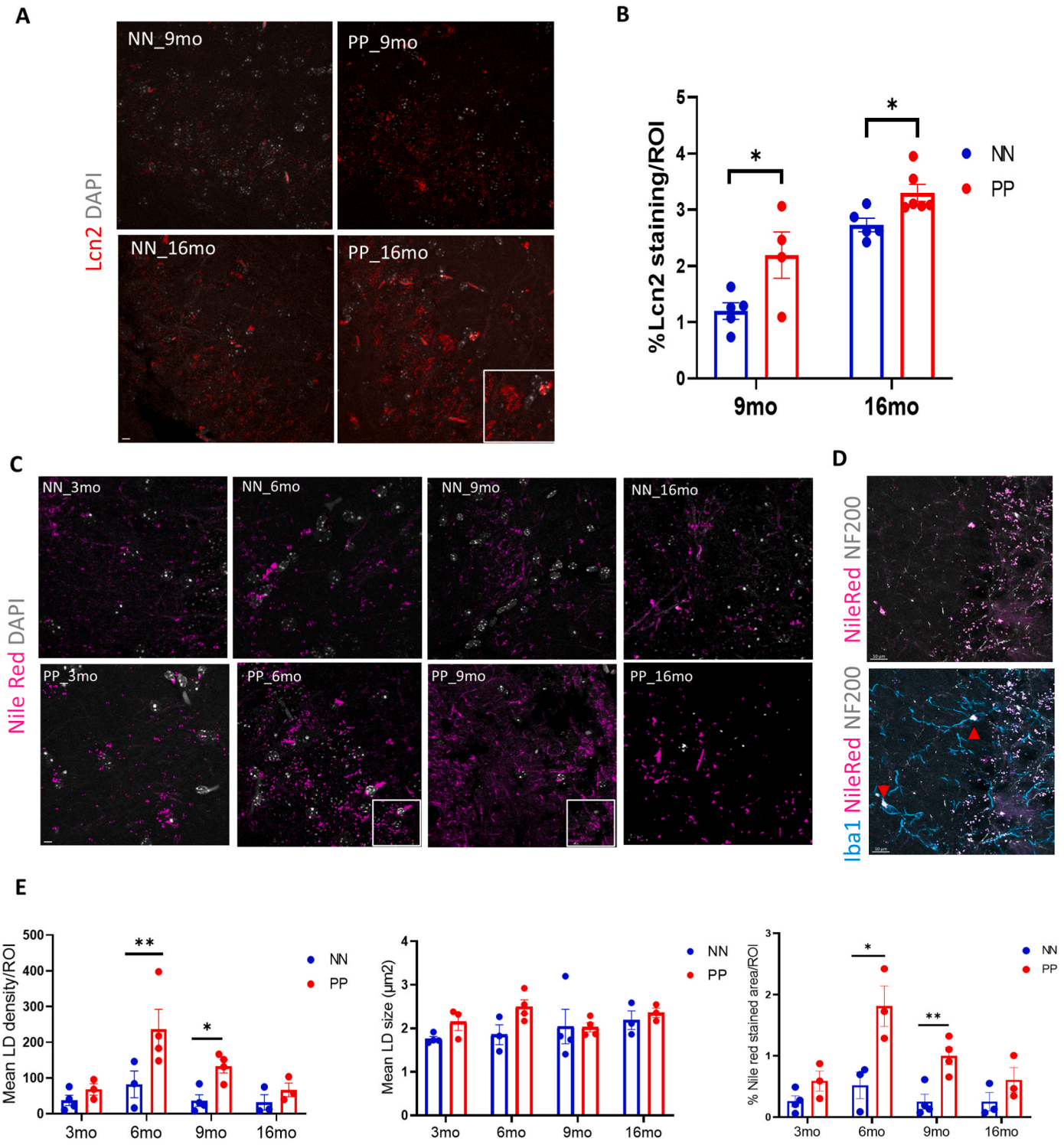

Fig. 6. Effect of PolyI:C on the hippocampal Lcn-2 & lipid droplet (LD) density. (A) Representative Lcn-2 stained confocal images of saline and PolyI:C treated mice in 9 months and 16 months aged PP mice. Larger aggregates of Lcn-2 (insert) visible at the 16 months PolyI:C exposed mice. **(B)** Quantification of % stained area indicates increased Lcn2 expression in the hippocampal CA3 field, *$p < 0.05$, two-way ANOVA followed with Holm-Sidak`s multiple comparison ($n = 4$–6 mice for 9 and 16-months groups/treatment). **(C)** Nile red positive lipid droplet staining (violet) across aging in NN & PP mice. Inserts showing aggregated lipid droplets **(D)** Representative triple fluorescence labeling with Nile Red, Iba1 (teal) and NF200 (grey) shows overlap between the different marker localized lipid droplets in Iba1 positive cells. Arrows indicating NileRed^{+}/Iba1^{+} cells. **(E)** Bar chart representing the lipid droplet (LD) density, mean size and % stained area per ROI measured. Data are represented as mean ± SEM ($n = 3$–4 mice per groups/treatment). *$p < 0.05$, **$p < 0.005$, two-way ANOVA, Fischer LSD. Scale bar A = 20 µm, C,E = 10 µm.

signaling genes, with specific repression in the PP model, we detect an opposite increasing trend in *c-Fos*, *c-Jun*, and *Notch1* to the PP model with a significant 3.1 upregulation of *c-Fos* in severe AD as compared to controls ($F_{2,21} = 3.2$ $p = 0.03$; Suppl. Table 7 and Fig. 7D). In the lipid metabolism group, *Plin4* and *Lcn2* show no change opposite to the PP model (Suppl. Table 7 and Fig. 7E), suggesting that those molecules are more implicated in vascular inflammation. To validate this assumption, we analyzed the vascular genes, *Klf4*, *Angptl4*, *Cyp1b1*, which showed

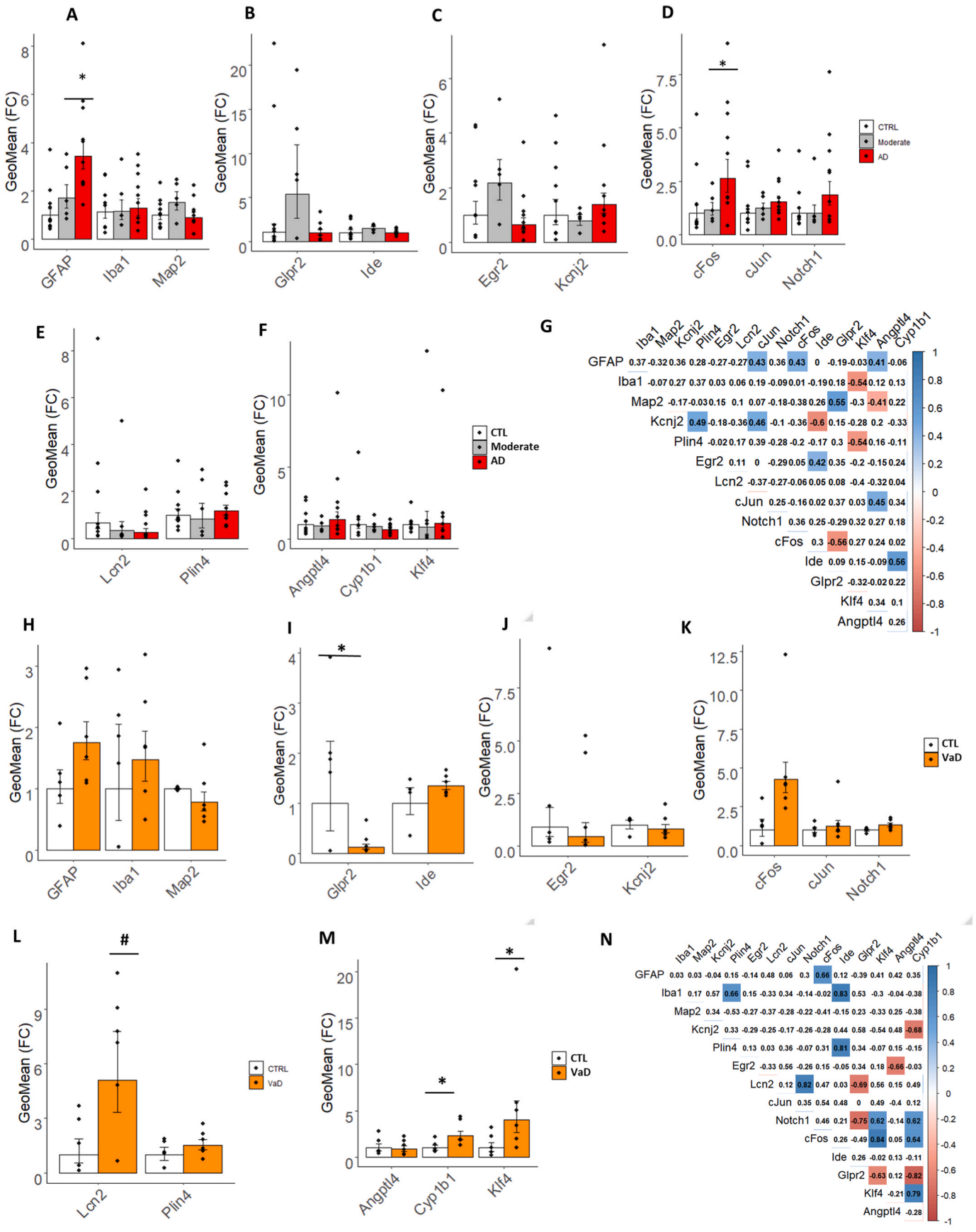

(caption on next page)

Fig. 7. Target transcripts validation in the human brain specimen of patients with AD and VaD. Bar plots with Jitter showing the fold changes (FC) of the DEGs (A–F) in moderate AD and severe AD entorhinal cortices as compared to healthy controls (CTRL) and (H–M) in hippocampal sections from VaD as compared to healthy controls (CTRL). (A and H) FC of cell-type specific markers for astroglia (GFAP), microglia (Iba1) and neurons (MAP2). (B and I) FC of glucose metabolism markers, Glpr2 and Ide. (C and J) FC of plasticity markers, Egr2 and Kcnj2. (D and K) FC of cell signaling markers, c-fos, c-Jun and Notch1. (E and L) FC of inflammatory and metabolic markers, Lcn2 and Plin4. (F and M). FC of vascular markers, Angptl4, Cyp1b1 and Klf4. (G and N) Correlation matrix of the selected biomarkers in the two study cohorts. Data are represented as Geometric mean of fold change ± Geometric SEM relative to healthy controls. *$p < 0.05$, #$p = 0.054$ based on one-way ANOVA/Bonferroni post hoc test correction. AD = Alzheimer's disease and VaD = vascular dementia.

transient alterations in the PP model, and observed no change across stages (Suppl. Table 7 and Fig. 7F). To understand the dependencies between the examined genes, we performed a correlation analysis using the aggregate population. In general, all interactions are moderately significant ($r > 0.5$) with positive associations between *c-fos* and *GFAP,* matching the increasing trend of the two transcripts, which suggests a cell-type-specific change, while *c-fos* is negatively associated with *Glpr2* (Fig. 7G). *Kcnj2* is inversely associated with *Ide* reflecting their opposite trend, while *Ide* is positively correlated with *Cyp1b1* (Fig. 7G), indicating potential dependencies. Other interactions among the studied genes are seen but too subtle to be of functional relevance. Overall, the PolyI:C model replicates some aspects of neurodegenerative dementia with increased tauopathy, microglia changes, the gene expression between the mouse and humans differs substantially, raising the possibility of a mixed-vascular-AD model with diverse genetic fingerprints.

3.8. Translation into vascular dementia

To verify any transcriptomic changes related to vascular dementia, we performed gene targets' validation on the second cohort of hippocampi from vascular dementia patients and age-matched healthy controls (Table 4 and Suppl. Table 2). Cell type-specific genes, *GFAP* and *Iba1*, indicate an increasing but not significant trend of microglia and astroglia, while MAP2 levels remain unchanged. Accordingly to our model, *Glpr2* decreases by 90% in vascular dementia as compared to controls ($F_{1,9} = 5.28$ $p = 0.039$; Fig. 7I and Suppl. Table 8) suggesting ongoing vascular hypoxia (Xie et al., 2018)). On the other hand, the inflammatory and vascular markers, *Lcn2* ($F_{1,9} = 4.96$ $p = 0.05$) and *Cyp1b1* ($F_{1,9} = 7.10$ $p = 0.03$) increase in vascular dementia as in the PP model (Fig. 7L and M and Suppl. Table 8). Opposite to the genetic expression in the mouse, *Klf4*, *Notch1,* and *c-fos* levels rise in vascular dementia (Fig. 7M and K and Suppl. Table 8). Correlation analysis of the differentially expressed genes in the aggregate cohort indicates a positive association ($r > 0.6$) among *Lcn2, Notch1, and Klf4*, implicating those factors in the vascular pathology. Whereas, along the mechanistic trajectory of vascular remodeling a negative association is observed between *Glpr2* and the two angiogenesis genes, *Klf4* and *Cyp1b1*. These results indicate that a handful of the gene targets that are significantly affected by systemic inflammation in the brain of PP mice are reproduced in vascular neurodegenerative dementia.

4. Discussion

4.1. Spread of peripheral inflammation to the brain

AD is a multifactorial complex disorder requiring the understanding of causal risk factors for proper treatment. Among those agents, microbial infections causing low-grade inflammatory responses over a lifetime are causally implicated in the development of AD with aging (Hammond et al., 2010; Miklossy et al., 2004; Dominy et al., 2019). Experiments in transgenic mice for APP and Tau animals using viral and bacterial derivatives, such as PolyI:C and Lipopolysaccharides (LPS), aggravate the pathophysiological progression of AD (Krstic et al., 2012; Kitazawa et al., 2005). Based on these findings, we postulated that PolyI:C sterile infections prenatally and postnatally in young adulthood may be a sufficient driver of AD-pathology as a result of sustained peripheral inflammation. Our cross-sectional and multi-modal examination of such an experimental model demonstrates that systemic infection with the double-stranded viral RNA surrogate, PolyI:C, causes the upregulation of circulating inflammatory humoral factors (MCP-1, IL-6, IL-10, and TNF-α) by 3 months of age which precedes the neuroinflammatory wave (IFN-γ, IL-6, IL-1β) occurring 3 months later. Despite no extravasation of neutrophils, monocytes or polymorphonuclear cells to the brains at 3 and 6 months, supporting an intact blood-brain barrier at these stages, cytokines of the innate and adaptive immunity can spread from the periphery to the brain triggering deleterious neuroinflammatory events. This is aligned with findings in humans where elevated IL-6 and IL-10 levels in the blood or brain of AD patients have been associated with the severity of cognitive decline and increased ventricular volume (Licastro et al., 2003; Leung et al., 2013). In parallel to the observed rise of neuroinflammation with aging, we also see an increase in microglia and astroglia gene expression at 6 and 9 months, reflecting cell-type-specific changes in these populations (Fig. 1). Interestingly, in the very old animals at 16 months the inflammatory tone dissipates suggesting a late immune deficiency attributed to immunosenescence upon low-grade chronic inflammation typical in infections (Pawelec et al., 2005; Furman et al., 2019).

4.2. Progressive tauopathy

Along with the rise in central inflammatory responses (IL-6 and IFN-γ), at 6 months of age PolyI:C brains display a rise in hippocampal tau phosphorylation supporting a causal link between IL-6 and tau hyperphosphorylation (p-Tau205/tau) as previously demonstrated in rat embryonic hippocampal neurons (Quintanilla 2004). In the aged PP mice, at 16 months, insoluble tangles are visible in the hippocampus as small neuropil aggregates internalized at times by astroglia cells and in vessels reflecting a CAA, likely contributing to its selective vulnerability (Stranahan and Mattson 2010) and the spatial reference memory deficit (Fyhn et al., 2004). Overall, the progressive tauopathy as a result of chronic neuroinflammation in PolyI:C mice disrupts neural networks' integrity affecting spatial memory encoding .

4.3. Microglia phenotypic change

Microglia are the major innate immune cells of the central nervous system mediating host defense responses against infectious agents, injury, abnormal accumulation of amyloid-β, and prion proteins (Yin et al., 2017). These cells express TLR3 viral receptors recognizing double-stranded RNA viruses (Town et al., 2006) and therefore play an important role in neuroinflammation in response to such stimuli initiating neuronal death. We have reported here a full-length characterization of microglial morphological changes across aging within the hippocampus of PolyI:C mice. We observe a typical pathological shift with aging from resting to intermediate hyper-ramification with larger soma and a strong reactive phagocytic morphology with fewer endpoints and branch lengths in the later stage (Walkera et al. 2013). In alignment with our study, others have reported an enlargement in the microglia soma/volume and a reduction in endpoints and branch length after bacterial LPS exposure (D'Aloia et al., 2021). As proposed earlier (Knuesel et al., 2014), the dynamic changes in the microglial morphology indicate a potential priming effect due to both maternal and early postnatal immune activation. In our study morphological changes in the aging PolyI:C mice resemble a microglial phenotype upon injury (Streit et al. 1999) and after acute inflammatory response with neuraminidase treatment (Fernández-Arjona et al., 2017). Despite the recent

evidence of a profoundly diverse genetic repertoire in rodents and human microglia (Masuda et al., 2019), the phenotypic transitions of microglia cells in this and other models recapitulate the dynamic undergoing changes during neuroinflammation. Our and other findings support that neuroinflammation, passed on by the circulation and in response to the proteinopathy, is perpetuated influencing microglia cell fate to acquire a synaptic- and neuro-toxic phenotype (Combs et al., 1999).

4.4. Genetic remodeling

To further support the use of the PolyI:C mouse model as a viable preclinical experimental animal for neurodegenerative research, we discovered alterations in the hippocampal transcriptome relevant to synaptic dysfunction, inflammation, and neurodegenerative dementia. GEA using the SynGO database indicates the biggest changes in presynaptic gene markers at the early stages (3 months), a steady-state at 6 months, and from 9 months on a progressive enrichment in postsynaptic genes. This is in line with the observed early presynaptic release of glutamate (Palop and Mucke 2010), followed in time by post-synaptic scaling events aimed at preserving neuronal integrity at the expense of synaptic transmission (Findley et al., 2019). This mechanistic progression is theoretically confirmed by an aggregate GEA using KEGG, Wikipathway, and Reactome pathways, which shows an early abundance in calcium signaling cascades, inflammation pathways, including MAPK signaling, PI3K-AKT signaling associated with cell survival and apoptosis. While at 6 months we confirmed an important decrease in *Glpr2* associated with synaptic depotentiation in response to hyperactivity (Sasaki-Hamada et al. 2019),(Xie et al., 2018; Bhusal et al., 2019), genes associated with neuroinflammation such as *Lcn2* and *Plin4* were increased at the late stages. *Lcn2* is a key gene involved in iron regulation and inflammation (Dekens et al., 2018). Lcn2 in neurons and glial cells generates neuroinflammatory responses (Bi et al., 2013) associated with insulin resistance and synaptic modulation (Song and Kim 2018) whereas accumulation in the endothelial barrier affects BBB permeability (Ferreira et al., 2015). Lcn-2 is upregulated during systemic inflammation (Kang et al., 2017) and is elevated in the brains of AD patients (Naudé et al., 2012). While, recent evidence indicates that Lcn-2 is a differential diagnosis marker for Vascular dementia, with increased brain and CSF Lcn-2 expression in vascular diseases in comparison with AD (Llorens et al., 2020a), the observed upregulation of Lcn-2 in post-mortem AD brains suggests that it may be a suitable druggable target in sporadic LOAD. On the other hand, *Plin4* is often associated with triacylglycerol metabolism and is involved in the biogenesis of lipid droplets in pathological degeneration (Han et al., 2018). The PolyI:C model shows a strong and specific rise in lipid droplets density accompanied by an increase in Lcn2 protein levels in neurons and glia, which confirms the metabolic and inflammatory imbalance. Interestingly, the origin of neurotoxic Lcn2 can be sourced back to astrocytes and increased levels of Lcn2 are seen in the brains of patients with human immunodeficiency virus 1 (HIV-1) reporting neurocognitive impairment (Ojeda-Juárez et al., 2020). Thus, Lcn-2 overexpression upon low-grade systemic inflammation supports its role as a putative druggable target to halt the immune-driven neuropathological progression.

4.5. Reproducibility in postmortem tissue from AD and vascular dementia patients

One of the challenges of understanding the physiopathology of AD to develop targetable therapeutics is partially attributed to the poor reproducibility between animal models and humans and the multifactorial etiology of the disease (Götz et al. 2018). Inflammatory, vascular processes and misfolded proteins should be considered as a whole and investigated closely to unravel dependencies. Furthermore, overlapping pathologies between AD and VaD, represent over 20% of the cases supporting common mechanisms and therapeutic avenues. Consistently, our study indicates that the PP model shows tauopathy coupled with a vascular deficit. This conclusion derives from our DEG target repertoire analysis in two cohorts representing i) progressive AD stages and ii) vascular dementia. We confirm astrogliosis in AD, captured by increased GFAP levels, comparable to the PP model. While this effect is present it is less pronounced in VaD. Interestingly, astrogliosis has been shown to increase proportionally to the extent of cognitive decline and is strongly associated with plaques and tangle formation (Serrano-Pozo et al., 2011). On the other hand, in VaD, astrogliosis and astroglial endfeet swelling has been implicated as one of the triggering factors for vascular damage (Price et al., 2018; Wang et al., 2018). In both instances, reactive astrogliosis is a commonality of the two diseases associated with the production of pro-inflammatory cytokines. Along with the increase in *GFAP* expression, we see a positive association with *c-fos* and *Notch1* levels in the severe AD stage, supporting the proliferation of astroglia (Hisanaga et al., 1990) and the role of Notch1 in driving astroglia proliferation in response to inflammation through the proto-oncogene *c-fos (Acaz-Fonseca* et al. *2019)*. This data is in opposition to the PP mouse model, where despite an increase in astroglia, a decline in *c-fos* and *Notch1* is observed at 9 months. The discrepancy can be explained by the different signaling profiles of glia and neurons in rodents, suggesting that cellular cascades may be cell-specific depending on the species.

Investigating the genes involved in mediating vascular function (Deniz et al. 2007), we observe no change in *Glpr2* expression in the progression of AD, while in VaD, *Glpr2* is downregulated similarly to the PP model supporting that cognitive deficit is contributed by lower blood perfusion (Xie et al., 2018). Along the same lines, the progressive increase in the inflammatory and metabolic markers, *Lcn2*, displayed by aging PP animals, is not reproduced in AD but the VaD specimen. This finding is in contrast to the previous reports of a rise in Lcn2 protein levels in the hippocampus of severe AD subjects (Naudé et al., 2012) and patients with MCI (Choi et al. 2011), but is in complete alignment with the recently reported upregulation of Lcn2 in cortex and CSF from VaD (Llorens et al., 2020b). In support of the microvessel damage mediated by Lcn2 (J.-H. Kim et al., 2017), 9 months old PP mice report a rise in *Cyp1b1*, *Angptl4,* and reduction in Klf4, which all regulate the BB permeability (Sangwung et al., 2017; Palenski et al., 2013; Huang et al., 2011) also seen in VaD specimen displaying increased *Cyp1b1, Klf4* transcripts. A vascular pathology in the PP model is supported by a two-fold reduction of Claudin 5, *Cldn5* (Suppl. Table 6), a key regulator of BBB permeability and an increase in lectin-stained microvasculature in the hippocampal CA3 field (Suppl. Fig. 6). Continuous high levels pro-inflammatory cytokines cause disruption of BBB's tight junction (TJ), resulting in downregulation of TJ proteins like Cldn5 and upregulation of angiogenic factors such as Angptl4 as already reported in various neuroinflammatory and neuroinfectious diseases caused by RNA viruses, including SARS-CoV-2 causing encephalitis (Bertrand et al. 2019; Salimi and Klein 2019; Leda et al., 2019; Altmayer et al., 2021). In this study, while the number of human samples analyzed is small, the translational validation of the PolyI:C data demonstrates that this mouse model can reproduce some of the characteristic features of reactive central inflammation (Hampel et al., 2020) and vascular pathology upon chronic infection, which resemble a glio-vascular phenotype of neurodegenerative dementia.

5. Conclusions

Overall, the present research, using a redesigned PolyI:C mouse model of sterile infection (Kristic et al., 2012), demonstrates that chronic systemic inflammation during adulthood causes progressive neuropathology with neuroinflammation, insoluble protein aggregates, vascular permeability, microglia remodeling, and behavioral deficits, mimicking vascular transcriptomic changes characteristic of Vascular AD. Although AD pre-clinical animal models are useful, one should acknowledge the limitations they possess in exhibiting the complete

pathology, complex and diverse etiology seen in AD, particularly when it comes to shared mixed vascular-AD. Our post-mortem analysis on AD and VaD brain specimens show partially overlapping genetic profiles between VaD and the PolyI:C mouse, which emphasizes the effect of systemic inflammation in causing vascular deficit besides neuroinflammation and tauopathy. Indeed, chronic inflammation is known to pose a risk for cardiovascular health which with aging may contribute to overlapping pathologies (Metti and Cauley 2012; Newcombe et al., 2018). This is further supported by recent evidence indicating that hyperphosphorylated tau can cause neurovascular decoupling (Park et al., 2020) bridging characteristic AD mechanisms to vascular deficits. Another important limitation of the current study is that we have not examined such anatomical or biochemical differences by sex as only male animals were included in this study. However, AD pathological hallmarks remain largely the same between both sexes (Yanguas-Casás 2020). Also, the precise mechanisms through which PolyI:C induces inflammation are inferred but not tested at this instance. Although a translational attempt has been made by validating selected transcriptional targets in AD and VaD brain specimens, the sample size is low, limiting its analytical power. Despite its limitations, this study provides insights into the role of systemic and CNS inflammation in mixed neurodegenerative pathologies, which are particularly important considering the long-term effects of neurotropic viral infections such as SARS-CoV-2 (Marshall 2021). The study is of use not only for the understanding of the interplay between peripheral and central processes underlying neurodegeneration but also presents a surrogate animal model for viral infectious pathologieslike COVID-19 during pregnancies and long-term effects of such infections during later life which is suitable for drug testing and preventive treatment.

Ethics approval and consent to participate

Animal experimentation was approved by the animal experiment committee, University of Fribourg (Protocol no. 2016_32_FR registered 01/01/2017).

The use of human tissue has been approved by the Ethical Commission of the Brain Bank for Dementia UK (OBB443 registered 1/05/2017 and OB344 registered 1/02/2014), Stanford (Stanford IRB), and the Ethical Commission from the Canton of Fribourg and Vaud (N. 325/14). All experiments conducted on human tissue comply with the WMA Declaration of Helsinki.

Consent for publication

All authors agree on publishing the original data.

Availability of data and materials

Supporting data is available in the form of supplementary material and tables. All raw data is available on request.

Funding

Schweizerischer Nationalfonds zur Förderung der Wissenschaftlichen Forschung (163470)(LA). Bundesbehörden der Schweizerischen Eidgenossenschaft (2017.0480) (PB).

Authors' contributions

PB conducted the main bulk of the experiments and wrote the manuscript. ID performed the bioinformatic analysis. EZ and ET performed cellular immunology experiments from blood and brain. AF and EB performed the blind quantitative analysis of microglia morphology using custom-made scripts. MAD assisted in the inflammatory model characterization. LA designed the study and wrote the manuscript. All authors read and approved the final manuscript.

Declaration of competing interest

There are no competing interests.

Data availability

Data will be made available on request.

Acknowledgements

We would like to thank Mrs. E. Martin and V. Tache for their technical support. We are also grateful to Dr. M. Reggente for providing his expertise in R. We thank Prof. T. Montine for sharing the brain tissue from the Stanford Biobank for this study. We are thankful to the donors and their families for allowing us access to the human tissue (Oxford, UK, and Stanford, USA).

Appendix A. Supplementary data

Supplementary data to this article can be found online at https://doi.org/10.1016/j.bbih.2022.100568.

References

Acaz-Fonseca, Estefania, Ortiz-Rodriguez, Ana, Azcoitia, Iñigo, Garcia-Segura, Luis M., Arevalo, Maria-Angeles, 2019. Notch signaling in astrocytes mediates their morphological response to an inflammatory challenge. Cell Death Discov. 5, 85. April.

Aikawa, Tomonori, Ren, Yingxue, Yamazaki, Yu, Tachibana, Masaya, Johnson, Madeleine R., Anderson, Casey T., Martens, Yuka A., et al., 2019. ABCA7 haplodeficiency disturbs microglial immune responses in the mouse brain. Proc. Natl. Acad. Sci. U.S.A. 116 (47), 23790–23796.

Altmayer, Victor, Ziveri, Jason, Frère, Corinne, Joe-Elie Salem, Weiss, Nicolas, Cao, Albert, Marois, Clémence, et al., 2021. Endothelial cell biomarkers in critically ill COVID-19 patients with encephalitis. J. Neurochem. https://doi.org/10.1111/jnc.15545. November.

Barber, Robert C., 2012. The genetics of Alzheimer's disease. *Scientifica* 2012 (December). https://doi.org/10.6064/2012/246210.

Bertrand, Luc, Velichkovska, Martina, Toborek, Michal, 2019. Cerebral vascular toxicity of antiretroviral therapy. J. Neuroimmune Pharmacol.: The Off. J. Soc. NeuroImmun. Pharmacol. https://doi.org/10.1007/s11481-019-09858-x. June.

Bhusal, Anup, Habibur Rahman, Md, Lee, In-Kyu, Suk, Kyoungho, 2019. Role of hippocampal lipocalin-2 in experimental diabetic encephalopathy. Front. Endocrinol. 10 https://doi.org/10.3389/fendo.2019.00025.

Bi, Fangfang, Huang, Cao, Tong, Jianbin, Qiu, Guang, Huang, Bo, Wu, Qinxue, Li, Fang, et al., 2013. Reactive astrocytes secrete lcn2 to promote neuron death. Proc. Natl. Acad. Sci. U.S.A. 110 (10), 4069–4074.

Bilbo, Staci D., Block, Carina L., Bolton, Jessica L., Hanamsagar, Richa, Tran, Phuong K., 2018. Beyond infection - maternal immune activation by environmental factors, microglial development, and relevance for autism spectrum disorders. Exp. Neurol. 299 (Pt A), 241–251.

Binda, Anna, Rivolta, Ilaria, Villa, Chiara, Chisci, Elisa, Beghi, Massimiliano, Cornaggia, Cesare M., Giovannoni, Roberto, Combi, Romina, 2018. A novel KCNJ2 mutation identified in an autistic proband affects the single channel properties of Kir2.1. Front. Cell. Neurosci. https://doi.org/10.3389/fncel.2018.00076.

Bindea, Gabriela, Mlecnik, Bernhard, Hubert, Hackl, Charoentong, Pornpimol, Tosolini, Marie, Amos, Kirilovsky, Fridman, Wolf-Herman, Pagès, Franck, Trajanoski, Zlatko, Galon, Jérôme, 2009. ClueGO: a cytoscape plug-in to decipher functionally grouped gene ontology and pathway annotation networks. Bioinformatics 25 (8), 1091–1093.

Brai, Emanuele, Alberi, Lavinia, 2015. Simple and computer-assisted olfactory testing for mice. JoVE 100, e52944. June.

Brai, Emanuele, Marathe, Swananda, Astori, Simone, Ben Fredj, Naila, Perry, Elisabeth, Lamy, Christophe, Scotti, Alessandra, Alberi, Lavinia, 2015. Notch1 regulates hippocampal plasticity through interaction with the reelin pathway, glutamatergic transmission and CREB signaling. Front. Cell. Neurosci. 9 (November), 447.

Carvey, Paul M., Chang, Qin, Lipton, Jack W., Ling, Zaodung, 2003. Prenatal exposure to the bacteriotoxin lipopolysaccharide leads to long-term losses of dopamine neurons in offspring: a potential, new model of Parkinson's disease. Front. Biosci.: J. Vis. Literacy 8, s826–s837. September.

Chakraborty, Ananya, Kamermans, Alwin, het Hof, Bert van, Castricum, Kitty, Aanhane, Ed, Horssen, Jack van, Thijssen, Victor L., et al., 2018. Angiopoietin like-4 as a novel vascular mediator in capillary cerebral amyloid Angiopathy. Brain. https://doi.org/10.1093/brain/awy274.

Chen, Yanting, Hong, Tingting, Chen, Feng, Sun, Yuanhong, Wang, Yan, Cui, Lili, 2021. Interplay between microglia and Alzheimer's disease—focus on the most relevant risks: APOE genotype, sex and age. Front. Aging Neurosci. 13 https://doi.org/10.3389/fnagi.2021.631827.

Choi, Jihye, Lee, Ho-Won, Suk, Kyoungho, 2011. Increased plasma levels of Lipocalin 2 in mild cognitive impairment. J. Neurol. Sci. 305 (1–2), 28–33.
Combs, Colin K., Johnson, Derrick E., Cannady, Steve B., Lehman, Timothy M., Landreth, Gary E., 1999. Identification of microglial signal transduction pathways mediating a neurotoxic response to amyloidogenic fragments of β-amyloid and prion proteins. J. Neurosci.: Off. J. Soc. Neurosci. 19 (3), 928–939.
Conway, Fiona, Brown, Alan S., 2019. Maternal immune activation and related factors in the risk of offspring psychiatric disorders. Front. Psychiatr./Front. Res. Found. 10 (June), 430.
Crawley, Jacqueline, Bailey, Kathleen, 2008. Anxiety-related behaviors in mice. Method Behav. Anal. Neurosci. https://doi.org/10.1201/noe1420052343.ch5. Second Edition.
Cunningham, Colm, 2013. Microglia and neurodegeneration: the role of systemic inflammation. Glia 61 (1), 71–90.
Cunningham, Colm, Hennessy, Edel, 2015. Co-morbidity and systemic inflammation as drivers of cognitive decline: new experimental models adopting a broader paradigm in dementia research. Alzheimer's Res. Ther. 7 (1), 1–13.
D'Aloia, Alessia, Molteni, Laura, Gullo, Francesca, Bresciani, Elena, Artusa, Valentina, Rizzi, Laura, Ceriani, Michela, et al., 2021. Palmitoylethanolamide modulation of microglia activation: characterization of mechanisms of action and implication for its neuroprotective effects. Int. J. Mol. Sci. 22 (6) https://doi.org/10.3390/ijms22063054.
Davis, Benjamin M., Salinas-Navarro, Manual, Francesca Cordeiro, M., Moons, Lieve, De Groef, Lies, 2017. Characterizing microglia activation: a spatial statistics approach to maximize information extraction. Sci. Rep. 7 (1), 1576.
De Chiara, Giovanna, Piacentini, Roberto, Fabiani, Marco, Mastrodonato, Alessia, Elena Marcocci, Maria, Limongi, Dolores, Napoletani, Giorgia, et al., 2019. Recurrent Herpes Simplex virus-1 infection induces hallmarks of neurodegeneration and cognitive deficits in mice. PLoS Pathog. 15 (3), e1007617.
Dekens, Doortje W., De Deyn, Peter P., Sap, Friederike, Eisel, Ulrich L.M., Naudé, Petrus J.W., 2020. Iron chelators inhibit amyloid-β-induced production of Lipocalin 2 in cultured astrocytes. Neurochem. Int. 132 (January), 104607.
Dekens, Doortje W., Naudé, Petrus J.W., Keijser, Jan N., Boerema, Ate S., De Deyn, Peter P., Eisel, Ulrich L.M., 2018. Lipocalin 2 contributes to brain iron dysregulation but does not affect cognition, plaque load, and glial activation in the J20 alzheimer mouse model. J. Neuroinflammation 15 (1), 330.
Deniz, Mustafa, Bozkurt, Ayhan, Kurtel, Hizir, 2007. Mediators of glucagon-like peptide 2-induced blood flow: responses in different vascular sites. Regul. Pept. 142 (1–2), 7–15.
Dominy, Stephen S., Lynch, Casey, Ermini, Florian, Benedyk, Malgorzata, Marczyk, Agata, Konradi, Andrei, Nguyen, Mai, et al., 2019. Porphyromonas Gingivalis in Alzheimer's disease brains: evidence for disease causation and treatment with small-molecule inhibitors. Sci. Adv. 5 (1), eaau3333.
Du, Yanjiao, Liu, Chao, Ma, Congmin, Xu, Xiaohui, Zhou, Xufeng, Zhou, Haitao, Huang, Chao, 2019. Cerebral amyloid angiopathy-related inflammation: a case report presenting with a rare variant in SORL1 gene. BMC Neurol. 19 (1), 97.
Engelhart, Marianne J., Geerlings, Mirjam I., Meijer, John, Kiliaan, Amanda, Ruitenberg, Annemieke, van Swieten, John C., Stijnen, Theo, Hofman, Albert, Jacqueline, C., Witteman, M., Breteler, Monique M.B., 2004. Inflammatory proteins in plasma and the risk of dementia: the rotterdam study. Arch. Neurol. 61 (5), 668–672.
Fernández-Arjona, María del Mar, Fernández-Arjona, María del Mar, Grondona, Jesús M., Granados-Durán, Pablo, Fernández-Llebrez, Pedro, López-Ávalos, María D., 2017. Microglia morphological categorization in a rat model of neuroinflammation by hierarchical cluster and principal components analysis. Front. Cell. Neurosci. https://doi.org/10.3389/fncel.2017.00235.
Ferreira, Ana C., Mesquita, Sandro Dá, Sousa, João C., Correia-Neves, Margarida, Sousa, Nuno, Palha, Joana A., Marques, Fernanda, 2015. From the periphery to the brain: lipocalin-2, a friend or foe? Prog. Neurobiol. https://doi.org/10.1016/j.pneurobio.2015.06.005.
Findley, Caleigh A., Bartke, Andrzej, Hascup, Kevin N., Hascup, Erin R., 2019. Amyloid beta-related alterations to glutamate signaling dynamics during Alzheimer's disease progression. ASN Neuro. https://doi.org/10.1177/1759091419855541.
Fitz, Nicholas F., Nyon Nam, Kyong, Wolfe, Cody M., Letronne, Florent, Playso, Brittany E., Iordanova, Bistra E., Kozai, Takashi D.Y., et al., 2021. Phospholipids of APOE lipoproteins activate microglia in an isoform-specific manner in preclinical models of Alzheimer's disease. Nat. Commun. 12 (1), 1–18.
Fulop, Tamas, Witkowski, Jacek M., Bourgade, Karine, Khalil, Abdelouahed, Zerif, Echarki, Larbi, Anis, Hirokawa, Katsuiku, et al., 2018. Can an infection hypothesis explain the beta amyloid hypothesis of Alzheimer's disease? Front. Aging Neurosci. 10 (July), 224.
Furman, David, Judith Campisi, Verdin, Eric, Carrera-Bastos, Pedro, Targ, Sasha, Claudio Franceschi, Ferrucci, Luigi, et al., 2019. Chronic inflammation in the etiology of disease across the life span. Nat. Med. 25 (12), 1822–1832.
Fyhn, Marianne, Molden, Sturla, Witter, Menno P., Moser, Edvard I., Moser, May-Britt, 2004. Spatial representation in the entorhinal cortex. Science 305 (5688), 1258–1264.
Ghosh, Chaitali, Hossain, Mohammed, Solanki, Jesal, Dadas, Aaron, Nicola Marchi, Janigro, Damir, 2016. Pathophysiological implications of neurovascular P450 in brain disorders. Drug Discov. Today. https://doi.org/10.1016/j.drudis.2016.06.004.
Giovanoli, Sandra, Notter, Tina, Richetto, Juliet, Labouesse, Marie A., Vuillermot, Stéphanie, Riva, Marco A., Meyer, Urs, 2015. Late prenatal immune activation causes hippocampal deficits in the absence of persistent inflammation across aging. J. Neuroinflammation 12 (November), 221.
Götz, Jürgen, Bodea, Liviu-Gabriel, Goedert, Michel, 2018. Rodent models for alzheimer disease. Nat. Rev. Neurosci. 19 (10), 583–598.
Greenspan, P., Mayer, E.P., Fowler, S.D., 1985. Nile red: a selective fluorescent stain for intracellular lipid droplets. J. Cell Biol. 100 (3), 965–973.
Hammond, Christine J., Hallock, Loretta R., Howanski, Raymond J., Appelt, Denah M., Scott Little, C., Balin, Brian J., 2010. Immunohistological detection of Chlamydia Pneumoniae in the Alzheimer's disease brain. BMC Neurosci. 11 (September), 121.
Hampel, Harald, Caraci, Filippo, Cuello, A. Claudio, Caruso, Giuseppe, Nisticò, Robert, Corbo, Massimo, Baldacci, Filippo, et al., 2020. A path toward precision medicine for neuroinflammatory mechanisms in Alzheimer's disease. Front. Immunol. 11 (March), 456.
Han, Xiaojuan, Zhu, Jialei, Zhang, Xinlei, Song, Qiqi, Ding, Jianhua, Lu, Ming, Sun, Sifan, Hu, Gang, 2018. Plin4-Dependent lipid droplets hamper neuronal mitophagy in the MPTP/p-Induced mouse model of Parkinson's disease. Front. Neurosci. https://doi.org/10.3389/fnins.2018.00397.
Hisanaga, K., Sagar, S.M., Hicks, K.J., Swanson, R.A., Sharp, F.R., 1990. C-fos proto-oncogene expression in astrocytes associated with differentiation or proliferation but not depolarization. Brain Res. Mol. Brain Res. 8 (1), 69–75.
Hoeijmakers, Lianne, Heinen, Yvonne, Anne-Marie van Dam, Lucassen, Paul J., Korosi, Aniko, 2016. Microglial priming and Alzheimer's disease: a possible role for (early) immune challenges and epigenetics? Front. Hum. Neurosci. https://doi.org/10.3389/fnhum.2016.00398.
Huang, Royston-Luke, Teo, Ziqiang, Chong, Han Chung, Zhu, Pengcheng, Tan, Ming Jie, Tan, Chek Kun, Ivan Lam, Chee Ren, et al., 2011. ANGPTL4 modulates vascular junction integrity by integrin signaling and disruption of intercellular VE-cadherin and claudin-5 clusters. Blood 118 (14), 3990–4002.
Hui, Chin W., St-Pierre, Abygaël, Hassan, El Hajj, Remy, Yvan, Hébert, Sébastien S., Luheshi, Giamal N., Srivastava, Lalit K., Tremblay, Marie-Ève, 2018. Prenatal immune challenge in mice leads to partly sex-dependent behavioral, microglial, and molecular abnormalities associated with schizophrenia. Front. Mol. Neurosci. 11 (February), 13.
Ito, Hiroshi T., Smith, Stephen E.P., Hsiao, Elaine, Patterson, Paul H., 2010. Maternal immune activation alters nonspatial information processing in the Hippocampus of the adult offspring. Brain Behav. Immun. 24 (6), 930–941.
Itzhaki, Ruth F., Wozniak, Matthew A., 2006. Herpes Simplex virus type 1, apolipoprotein E, and cholesterol: a dangerous liaison in Alzheimer's disease and other disorders. Prog. Lipid Res. 45 (1), 73–90.
Jha, Mithilesh Kumar, Lee, Shinrye, Park, Dong Ho, Kook, Hyun, Park, Keun-Gyu, Lee, In-Kyu, Suk, Kyoungho, 2015. Diverse functional roles of lipocalin-2 in the central nervous system. Neurosci. Biobehav. Rev. 49 (February), 135–156.
Kang, S.S., Ren, Y., Liu, C.-C., Kurti, A., Baker, K.E., Bu, G., Asmann, Y., Fryer, J.D., 2017. Lipocalin-2 protects the brain during inflammatory conditions. Mol. Psychiatr. 23 (2), 344–350.
Kim, Eun Kyung, Choi, Eui-Ju, 2010. Pathological roles of MAPK signaling pathways in human diseases. Biochim. Biophys. Acta 1802 (4), 396–405.
Kim, Jae-Hong, Ko, Pan-Woo, Lee, Ho-Won, Jeong, Ji-Young, Lee, Maan-Gee, Kim, Jong-Heon, Lee, Won-Ha, Yu, Ri, Oh, Won-Jong, Suk, Kyoungho, 2017. Astrocyte-derived lipocalin-2 mediates hippocampal damage and cognitive deficits in experimental models of vascular dementia. Glia 65 (9), 1471–1490.
Kitazawa, Masashi, Salvatore, Oddo, Yamasaki, Tritia R., Green, Kim N., LaFerla, Frank M., 2005. Lipopolysaccharide-Induced inflammation exacerbates tau pathology by a cyclin-dependent kinase 5-mediated pathway in a transgenic model of Alzheimer's disease. J. Neurosci.: Off. J. Soc. Neurosci. 25 (39), 8843–8853.
Knuesel, Irene, Chicha, Laurie, Britschgi, Markus, Schobel, Scott A., Bodmer, Michael, Hellings, Jessica A., Stephen, Toovey, Prinssen, Eric P., 2014. Maternal immune activation and abnormal brain development across CNS disorders. Nat. Rev. Neurol. 10 (11), 643–660.
Koopmans, Frank, van Nierop, Pim, Andres-Alonso, Maria, Byrnes, Andrea, Cijsouw, Tony, Coba, Marcelo P., Cornelisse, L.Niels, et al., 2019. SynGO: an evidence-based, expert-curated knowledge base for the synapse. Neuron 103 (2), 217–234 e4.
Krstic, Dimitrije, Madhusudan, Amrita, Jana, Doehner, Vogel, Prisca, Notter, Tina, Imhof, Claudine, Manalastas, Abigail, et al., 2012. Systemic immune challenges trigger and drive alzheimer-like neuropathology in mice. J. Neuroinflammation 9 (July), 151.
Leda, Ana Rachel, Bertrand, Luc, Andras, Ibolya Edit, El-Hage, Nazira, Nair, Madhavan, Toborek, Michal, 2019. Selective disruption of the blood–brain barrier by zika virus. Front. Microbiol. https://doi.org/10.3389/fmicb.2019.02158.
Lee, Myoung-Hwa, Daniel, P. Perl, Nair, Govind, Li, Wenxue, Maric, Dragan, Murray, Helen, Dodd, Stephen J., et al., 2021. Microvascular injury in the brains of patients with covid-19. N. Engl. J. Med. 384 (5), 481–483.
Leung, Rufina, Proitsi, Petroula, Simmons, Andrew, Lunnon, Katie, Güntert, Andreas, Kronenberg, Deborah, Pritchard, Megan, et al., 2013. Inflammatory proteins in plasma are associated with severity of Alzheimer's disease. PLoS One 8 (6), e64971.
Licastro, Federico, Edoardo Grimaldi, Luigi Maria, Bonafè, Massimiliano, Martina, Chiappelli, Olivieri, Fabiola, Cavallone, Luca, Giovanietti, Simona, Masliah, Eliezer, Franceschi, Claudio, 2003. Interleukin-6 gene alleles affect the risk of Alzheimer's disease and levels of the cytokine in blood and brain. Neurobiol. Aging 24 (7), 921–926.
Li, Jun-Wei, Yu, Zong, Cao, Xi-Peng, Tan, Lin, Tan, Lan, 2018. Microglial priming in Alzheimer's disease. Ann. Transl. Med. 6 (10), 176.
Linard, Morgane, Letenneur, Luc, Garrigue, Isabelle, Angélique, Doize, Dartigues, Jean-François, Helmer, Catherine, 2020. Interaction between APOE4 and Herpes Simplex virus type 1 in Alzheimer's disease. Alzheimer's Dementia: The J. Alzheimer's Assoc. 16 (1), 200–208.
Ling, E.A., Wong, W.C., 1993. The origin and nature of ramified and amoeboid microglia: a historical review and current concepts. Glia 7 (1), 9–18.

Lin, Yen-Feng, Vernon Smith, Albert, Aspelund, Thor, Betensky, Rebecca A., Smoller, Jordan W., Gudnason, Vilmundur, Launer, Lenore J., Blacker, Deborah, 2019. Genetic overlap between vascular pathologies and Alzheimer's dementia and potential causal mechanisms. Alzheimer's Dementia: The J. Alzheimer's Assoc. 15 (1), 65–75.

Little, C. Scott, Hammond, Christine J., MacIntyre, Angela, Balin, Brian J., Appelt, Denah M., 2004. Chlamydia Pneumoniae induces alzheimer-like amyloid plaques in brains of BALB/c mice. Neurobiol. Aging 25 (4), 419–429.

Llorens, Franc, Hermann, Peter, Villar-Piqué, Anna, Diaz-Lucena, Daniela, Nägga, Katarina, Hansson, Oskar, Santana, Isabel, et al., 2020a. Cerebrospinal fluid Lipocalin 2 as a novel biomarker for the differential diagnosis of vascular dementia. Nat. Commun. 11 (1), 619.

Llorens, Franc, Hermann, Peter, Villar-Piqué, Anna, Diaz-Lucena, Daniela, Nägga, Katarina, Hansson, Oskar, Santana, Isabel, et al., 2020b. Cerebrospinal fluid Lipocalin 2 as a novel biomarker for the differential diagnosis of vascular dementia. Nat. Commun. 11 (1), 619.

Marshall, Michael, 2021. COVID and the brain: researchers zero in on how damage occurs. Nature 595 (7868), 484–485.

Masuda, Takahiro, Roman, Sankowski, Staszewski, Ori, Böttcher, Chotima, Sagar, Lukas Amann, Scheiwe, Christian, et al., 2019. Spatial and temporal heterogeneity of mouse and human microglia at single-cell resolution. Nature 566 (7744), 388–392.

McHugh, Stephen B., Niewoehner, Burkhard, Rawlins, J.N.P., Bannerman, David M., 2008. Dorsal hippocampal N-Methyl-D-Aspartate receptors underlie spatial working memory performance during non-matching to place testing on the T-maze. Behav. Brain Res. 186 (1), 41–47.

Metti, Andrea L., Cauley, Jane A., 2012. How predictive of dementia are peripheral inflammatory markers in the elderly? Neurodegener. Dis. Manag. 2 (6), 609–622.

Miedel, Christian J., Patton, Jennifer M., Miedel, Andrew N., Miedel, Edward S., Levenson, Jonathan M., 2017. Assessment of spontaneous alternation, novel object recognition and limb clasping in transgenic mouse models of amyloid-β and tau neuropathology. JoVE 123 (May). https://doi.org/10.3791/55523.

Miklossy, Judith, Khalili, Kamel, Gern, Lise, Ericson, Rebecca L., Darekar, Pushpa, Bolle, Lorie, Jean, Hurlimann, Bruce, J., Paster, 2004. Borrelia burgdorferi persists in the brain in chronic lyme neuroborreliosis and may Be associated with alzheimer disease. J. Alzheim. Dis.: JAD 6 (6), 639–649 discussion 673–81.

Moore, Zachery, Taylor, Juliet M., Crack, Peter J., 2019. The involvement of microglia in Alzheimer's disease: a new dog in the fight. Br. J. Pharmacol. 176 (18), 3533.

Morgan, Angharad R., Touchard, Samuel, Leckey, Claire, O'Hagan, Caroline, Alejo, J., Nevado-Holgado, , NIMA Consortium, Barkhof, Frederik, et al., 2019. Inflammatory biomarkers in Alzheimer's disease plasma. Alzheimer's Dementia: The J. Alzheimer's Assoc. 15 (6), 776–787.

Naudé, Petrus J.W., Nyakas, Csaba, Eiden, Lee E., Ait-Ali, Djida, van der Heide, Ragna, Engelborghs, Sebastiaan, Luiten, Paul G.M., De Deyn, Peter P., den Boer, Johan A., Eisel, Ulrich L.M., 2012. Lipocalin 2: novel component of proinflammatory signaling in Alzheimer's disease. Faseb. J. 26 (7), 2811.

Newcombe, Estella A., Camats-Perna, Judith, Silva, Mallone L., Valmas, Nicholas, , Tee Jong Huat, Medeiros, Rodrigo, 2018. Inflammation: the link between comorbidities, genetics, and Alzheimer's disease. J. Neuroinflammation 15 (1), 276.

Ojeda-Juárez, Daniel, Shah, Rohan, , Jerel Adam Fields, Harahap-Carrillo, Indira S., Koury, Jeffrey, Maung, Ricky, Gelman, Benjamin B., Baaten, Bas J., Roberts, Amanda J., Kaul, Marcus, 2020. Lipocalin-2 mediates HIV-1 induced neuronal injury and behavioral deficits by overriding CCR5-dependent protection. Brain Behav. Immun. 89 (October), 184–199.

Palenski, Tammy L., Sorenson, Christine M., Jefcoate, Colin R., Nader, Sheibani., 2013. Lack of Cyp1b1 promotes the proliferative and migratory phenotype of perivascular supporting cells. Labor. Investig. J. Tech. Method Pathol. 93 (6), 646–662.

Palop, Jorge J., Lennart, Mucke., 2010. Amyloid-β–induced neuronal dysfunction in Alzheimer's disease: from synapses toward neural networks. Nat. Neurosci. 13 (7), 812–818.

Park, Laibaik, Hochrainer, Karin, Hattori, Yorito, Ahn, Sung Ji, Antoine, Anfray, Wang, Gang, Uekawa, Ken, et al., 2020. Tau induces PSD95-neuronal NOS uncoupling and neurovascular dysfunction independent of neurodegeneration. Nat. Neurosci. 23 (9), 1079–1089.

Pawelec, Graham, Akbar, Arne, Caruso, Calogero, Solana, Rafael, Grubeck-Loebenstein, Beatrix, Anders, Wikby, 2005. Human immunosenescence: is it infectious? Immunol. Rev. 205 (June), 257–268.

Perry, V. Hugh, Cunningham, Colm, Holmes, Clive, 2007. Systemic infections and inflammation affect chronic neurodegeneration. Nat. Rev. Immunol. 7 (2), 161–167.

Pioli, Elsa Y., Gaskill, Brianna N., Gilmour, Gary, Tricklebank, Mark D., Dix, Sophie L., Bannerman, David, Garner, Joseph P., 2014. An automated maze task for assessing hippocampus-sensitive memory in mice. Behav. Brain Res. 261 (100), 249.

Price, Brittani R., Norris, Christopher M., Sompol, Pradoldej, Wilcock, Donna M., 2018. An emerging role of astrocytes in vascular contributions to cognitive impairment and dementia. J. Neurochem. 144 (5), 644–650.

Qiu, Wei Qiao, Folstein, Marshal F., 2006. Insulin, insulin-degrading enzyme and amyloid-beta peptide in Alzheimer's disease: review and hypothesis. Neurobiol. Aging 27 (2), 190–198.

Quintanilla, 2004. Interleukin-6 induces alzheimer-type phosphorylation of tau protein by deregulating the cdk5/p35 pathway. Exp. Cell Res. 295 (1), 245–257.

Rice, Rachel A., Berchtold, Nicole C., Cotman, Carl W., Green, Kim N., 2014. Age-related downregulation of the CaV3.1 T-type calcium channel as a mediator of amyloid beta production. Neurobiol. Aging 35 (5), 1002–1011.

Saeed, Sadia, Quintin, Jessica, Kerstens, Hindrik H.D., Rao, Nagesha A., Ali, Aghajanirefah, Matarese, Filomena, Cheng, Shih-Chin, et al., 2014. Epigenetic programming of monocyte-to-macrophage differentiation and trained innate immunity. Science 345 (6204), 1251086.

Salimi, Hamid, Klein, Robyn S., 2019. Disruption of the blood-brain barrier during neuroinflammatory and neuroinfectious diseases. In: Neuroimmune Diseases: from Cells to the Living Brain Hiroshi Mitoma and Mario Manto, 195–234. Springer International Publishing, Cham.

Sangwung, Panjamaporn, Zhou, Guangjin, Lalitha Nayak, E., Chan, Ricky, Kumar, Sandeep, Kang, Dong-Won, Zhang, Rongli, 2017. et al KLF2 and KLF4 Control Endothelial Identity and Vascular Integrity. JCI Insight 2 (4), e91700.

Sankowski, Roman, Mader, Simone, Iván Valdés-Ferrer, Sergio, 2015. Systemic inflammation and the brain: novel roles of genetic, molecular, and environmental cues as drivers of neurodegeneration. Front. Cell. Neurosci. 9, 28. February.

Santos, Cláudia Y., Snyder, Peter J., Wu, Wen-chih, Zhang, Mia, Echeverria, Ana, Alber, Jessica, 2017. Pathophysiologic Relationship between Alzheimer's Disease, Cerebrovascular Disease, and Cardiovascular Risk: A Review and Synthesis." *Alzheimer's & Dementia: Diagnosis, Assessment & Disease Monitoring*. https://doi.org/10.1016/j.dadm.2017.01.005.

Sasaki-Hamada, Sachie, Ikeda, Masaatsu, Oka, Jun-Ichiro, 2019. Glucagon-like peptide-2 rescues memory impairments and neuropathological changes in a mouse model of dementia induced by the intracerebroventricular administration of streptozotocin. Sci. Rep. https://doi.org/10.1038/s41598-019-50167-3.

Serrano-Pozo, Alberto, Mielke, Matthew L., Gómez-Isla, Teresa, Betensky, Rebecca A., Growdon, John H., Frosch, Matthew P., Hyman, Bradley T., 2011. Reactive glia not only associates with plaques but also parallels tangles in Alzheimer's disease. Am. J. Pathol. 179 (3), 1373–1384.

Silveira, Vivian T., Castro Medeiros, Daniel, Ropke, Jivago, Guidine, Patricia A., Rezende, Gustavo H., Moraes, Marcio Flavio D., Eduardo Mazoni, A., Macedo, Danielle, Moreira, Fabricio A., Oliveira, Antonio Carlos P., 2017. Effects of early or late prenatal immune activation in mice on behavioral and neuroanatomical abnormalities relevant to schizophrenia in the adulthood. Int. J. Dev. Neurosci. https://doi.org/10.1016/j.ijdevneu.2017.01.009.

Sipilä, Pyry N., Heikkilä, Nelli, Lindbohm, Joni V., Hakulinen, Christian, Vahtera, Jussi, Elovainio, Marko, Suominen, Sakari, et al., 2021. Hospital-treated infectious diseases and the risk of dementia: a large, multicohort, observational study with a replication cohort. Lancet Infect. Dis. 21 (11), 1557–1567.

Sochocka, Marta, Zwolińska, Katarzyna, Leszek, Jerzy, 2017. The infectious etiology of Alzheimer's disease. Curr. Neuropharmacol. 15 (7), 996–1009.

Song, Juhyun, Kim, Oh Yoen, 2018. Perspectives in lipocalin-2: emerging biomarker for medical diagnosis and prognosis for Alzheimer's disease. Clin. Nutr. Res. https://doi.org/10.7762/cnr.2018.7.1.1.

Søraas, Arne, Ragnhild, Bø, Kalleberg, Karl Trygve, Støer, Nathalie C., Ellingjord-Dale, Merete, Landrø, Nils Inge, 2021. Self-reported memory problems 8 Months after COVID-19 infection. JAMA Netw. Open 4 (7), e2118717–e2118717.

Stranahan, Alexis M., Mattson, Mark P., 2010. Selective vulnerability of neurons in layer II of the entorhinal cortex during aging and Alzheimer's disease. Neural Plastic. 2010, 108190. December.

Streit, Wolfgang J., Walter, Sharon A., Pennell, Nathan A., 1999. Reactive microgliosis. Prog. Neurobiol. https://doi.org/10.1016/s0301-0082(98)00069-0.

Streit, Wolfgang J., Sammons, Nicole W., Kuhns, Amanda J., Larry Sparks, D., 2004. Dystrophic microglia in the aging human brain. Glia 45 (2), 208–212.

Tejera, Dario, Mercan, Dilek, Sanchez-Caro, Juan M., Hanan, Mor, Greenberg, David, Soreq, Hermona, Latz, Eicke, Douglas, Golenbock, Heneka, Michael T., 2019. Systemic inflammation impairs microglial Aβ clearance through NLRP3 inflammasome. EMBO J. 38 (17), e101064.

Thal, Dietmar Rudolf, Ghebremedhin, Estifanos, Udo, Rüb, Yamaguchi, Haruyasu, Tredici, Kelly Del, Braak, Heiko, 2002. Two types of sporadic cerebral amyloid Angiopathy. JNEN (J. Neuropathol. Exp. Neurol.) 61 (3), 282–293.

Ting, Jenny, 2001. Faculty Opinions Recommendation of Recognition of Double-Stranded RNA and Activation of NF-kappaB by Toll-like Receptor 3. Faculty Opinions – Post-Publication Peer Review of the Biomedical Literature. https://doi.org/10.3410/f.1001215.16876.

Toledo, Jon B., Arnold, Steven E., Raible, Kevin, Brettschneider, Johannes, Xie, Sharon X., Grossman, Murray, Monsell, Sarah E., Kukull, Walter A., Trojanowski, John Q., 2013. Contribution of cerebrovascular disease in autopsy confirmed neurodegenerative disease cases in the national Alzheimer's coordinating Centre. Brain. https://doi.org/10.1093/brain/awt188.

Town, Terrence, Jeng, David, Alexopoulou, Lena, Tan, Jun, Flavell, Richard A., 2006. Microglia recognize double-stranded RNA via TLR3. J. Immunol. 176 (6), 3804–3812.

Tzeng, Nian-Sheng, Chung, Chi-Hsiang, Lin, Fu-Huang, Chiang, Chien-Ping, Yeh, Chin-Bin, Huang, San-Yuan, Lu, Ru-Band, et al., 2018. Anti-herpetic medications and reduced risk of dementia in patients with Herpes Simplex virus infections—a nationwide, population-based cohort study in taiwan. Neurotherapeutics: The J. Am. Soc. Exp. NeuroTher. 15 (2), 417–429.

Van Hove, Hannah, Martens, Liesbet, Scheyltjens, Isabelle, De Vlaminck, Karen, Pombo Antunes, Ana Rita, De Prijck, Sofie, Vandamme, Niels, et al., 2019. A single-cell atlas of mouse brain macrophages reveals unique transcriptional identities shaped by ontogeny and tissue environment. Nat. Neurosci. 22 (6), 1021–1035.

Walkera, Rohan, Frederick, Nilsson, Michael, Jones, Kimberley, 2013. Acute and chronic stress-induced disturbances of microglial plasticity, phenotype and function. Curr. Drug Targets 14, 1262. October.

Wang, Feixue, Cao, Yu, Ma, Lina, Pei, Hui, Rausch, Wolf Dieter, Li, Hao, 2018. Dysfunction of cerebrovascular endothelial cells: prelude to vascular dementia. Front. Aging Neurosci. 10, 376. November.

Williams, J., Dragunow, M., Lawlor, P., Mason, S., Abraham, W.C., Leah, J., Bravo, R., Demmer, J., Tate, W., 1995. Krox20 may play a key role in the stabilization of long-term potentiation. Brain Res. Mol. Brain Res. 28 (1), 87–93.

Xie, Yan-Chun, Yao, Zhao-Hui, Yao, Xiao-Li, Pan, Jian-Zhen, Zhang, Shao-Feng, Zhang, Yong, Hu, Ji-Chang, 2018. Glucagon-like peptide-2 receptor is involved in spatial cognitive dysfunction in rats after chronic cerebral hypoperfusion. J. Alzheim. Dis.: JAD 66 (4), 1559–1576.

Yanguas-Casás, Natalia, 2020. Physiological sex differences in microglia and their relevance in neurological disorders. Neuroimmunol. Neuroinflammation 7, 13–22.

Yin, Jie, Valin, Katherine L., Dixon, Michael L., Leavenworth, Jianmei W., 2017. The role of microglia and macrophages in CNS homeostasis, autoimmunity, and cancer. J. Immunol. Res. https://doi.org/10.1155/2017/5150678, 2017 (December).

Young, Kimberly, Morrison, Helena, 2018. Quantifying microglia morphology from photomicrographs of immunohistochemistry prepared tissue using ImageJ. JoVE. https://doi.org/10.3791/57648.

Zhou, Yadi, Xu, Jielin, Hou, Yuan, Leverenz, James B., Kallianpur, Asha, Mehra, Reena, Liu, Yunlong, et al., 2021. Network medicine links SARS-CoV-2/COVID-19 infection to brain microvascular injury and neuroinflammation in dementia-like cognitive impairment. Alzheimer's Res. Ther. 13 (1), 1–19.

Sierra, Amanda, Andres C. Gottfried-Blackmore, Bruce S. McEwen, and Karen Bulloch. 2007. "Microglia Derived from Aging Mice Exhibit an Altered Inflammatory Profile." Glia 55 (4): 412–24.

Bennett, Rachel E., Ashley B. Robbins, Miwei Hu, Xinrui Cao, Rebecca A. Betensky, Tim Clark, Sudeshna Das, and Bradley T. Hyman. 2018. "Tau Induces Blood Vessel Abnormalities and Angiogenesis-Related Gene Expression in P301L Transgenic Mice and Human Alzheimer's Disease." Proceedings of the National Academy of Sciences of the United States of America 115 (6): E1289–98.

Tremblay, Sophie, Khalil Miloudi, Samaneh Chaychi, Sandra Favret, François Binet, Anna Polosa, Pierre Lachapelle, Sylvain Chemtob, and Przemyslaw Sapieha. 2013. "Systemic Inflammation Perturbs Developmental Retinal Angiogenesis and Neuroretinal Function." Investigative Ophthalmology & Visual Science 54 (13): 8125–39.